

# Biomedical evaluation of magnesium based biodegradable osteosynthesis implants

---

*MSc Thesis - Biomedical Engineering*  
*Malavika Nambiar*



 **TU Delft**

Delft University of Technology

**ETH** zürich



# Biomedical evaluation of magnesium based biodegradable osteosynthesis implants

by

Malavika Nambiar

to obtain the degree of Master of Science  
at the Delft University of Technology,  
to be defended publicly on Friday August 30, 2019 at 2 PM.

Student number: 4726944

Project duration: January 1, 2019 – July 31, 2019

Thesis committee: Assoc. Prof. dr. J. Zhou, TU Delft, supervisor  
Dr. L. Berger, ETH Zürich, supervisor  
Dr. L. Angeloni, TU Delft  
Dr. H. D. Besten, TU Delft

An electronic version of this thesis is available at <http://repository.tudelft.nl/>.





# Acknowledgement

The completion of this study was possible due to the contribution of many people and I am extremely grateful to each and every one of them for their unwavering support. My daily supervisor, Dr. Leopold Berger's encouragement, patience, support and edification has been the driving force that made me not only capable, but also enjoy the process of a master thesis. Prof. Löffler's encouragement, support and acceptance helped me take my project from the LMPT labs to the biological setting which has added much value to this thesis. My sincere thanks to the CABMM platform and Dr. Salim Darwiche for acting as my supervisor in the biological setting of the project, for training me and for many interesting discussions. My special thanks here to Dr. Flurina Clement for also training me in the lab and helpful discussions to plan experiments. The collaborators of this project, Dr. Thomas Steffen and Dr. Benoit Schaller have provided important feedback and helped to formulate the initial problem statement of this thesis and I am extremely grateful for their inputs. I would like to express my heartfelt appreciation to Prof. Jie Zhou who has supported me not only in the course of the master thesis, but also before. The moral support, encouragement and scientific inputs I received from him have played a pivotal role in the shaping of my thinking. I am thankful to all my colleagues at LMPT group for creating a conducive environment for learning and here I'd like to specially thank, Sebastian Reitz for manufacturing the various parts needed for my experiments, all so exceptionally well. A special thanks to Ayushman Talwar and Hande Eyisoğlu for their help and expert opinion on the creative graphics. It was possible for me to undertake this project in ETH Zurich only because of the financial support I received from the Idea league foundation and I am extremely grateful for this support. Finally, my deepest gratitude to my friends and family who have been extremely understanding, patient, supportive and made many sacrifices to help me with the course of my master studies. The encouragement, love and support I received from all these people gave me the strength to take upon this journey and to successfully complete it.

*Malavika Nambiar*  
*Zürich, August 2019*



# Abstract

Biodegradable materials such as polymers and magnesium and its alloys are gaining attention and approval for clinical use as osteosynthesis implants. However, polymers often lack the required mechanical strength and commercial Mg systems contain elements that are not naturally occurring in the body. Extra-high purity magnesium alloyed with 1 weight % zinc and 0.3 weight % calcium (ZX10) aims to confront these disadvantages to eventually emerge as an optimal material for fracture fixation.

In this thesis, ZX10 has been biomedically characterized using various tools to test its ability to function as a screw plate system in mandibular angle fractures. The material was analyzed after production using metallography techniques. Implants were designed and optimized using finite element techniques and mechanical tests were performed to compare strength against commercially available screw-plate Ti systems of the craniomaxillofacial (CMF) region. Cytotoxicity tests were undertaken to gain an insight into biocompatibility. All results indicate that ZX10 bone plate and screw can be designed within acceptable dimensions to match the flexural strength of a Ti plate in 4 point bending and a Ti screw in pull out tests. Cell cultures in 10 % concentrations of corrosion products show low cytotoxicity, 50 % concentrations show moderate cytotoxicity and 100 % concentrations of corrosion products show severe cytotoxicity. Viable cells were observed in the presence of the implant material.

With a corrosion rate of 1.08 mm/year in simulated body fluid, ZX10 behaves comparably to commercially available degradable systems such as the WE43 alloy and thus bespeaks further development and *in vivo* characterization to move towards clinical implementation.



# Extended Abstract



Graphical representation of the methods undertaken to biomedically characterize the ZX10 alloy for fixation of mandibular angle fractures.

Fracture fixation is moving towards biodegradable fixation methods to avoid second surgery associated with current gold standard devices. However, the biggest challenge in degradable fixation devices is the biocompatibility of the degrading products and the mechanical strength of the device. Keeping these problems in mind, this thesis project tests a novel extra-high purity magnesium alloy containing 1 % zinc and 0.3 % calcium (ZX10) by weight, all naturally occurring in the human body, for application as a screw plate system to achieve fixation in mandibular angle fractures.

The project focuses on material characterization, implant design, mechanical tests and cytotoxicity tests to bring initial insights into the envisioned application.

Metallography techniques were used to analyze the microstructure of the raw material which gives

an insight into the strength, ductility and structural homogeneity and to ensure product uniformity. The raw material with the highest volume fraction of recrystallization (91.7 % for screw material and 89.87 % for plate material) was deemed fit to manufacture the implants.

Plates and screws were designed based on recommendations from a craniomaxillofacial (CMF) surgeon, using Autodesk® Inventor® Professional software. The screw was designed to achieve a comparable pull out strength to a Ti screw, in artificial bone. This was validated experimentally by comparing pull out force normalized to the insertion depth. The ZX10 screws (n= 7) recorded a mean of 71.26 N/mm with a standard deviation of  $\pm 10.27$  and Ti screws (n= 6) recorded a mean of 40.97 N/mm with a standard deviation of  $\pm 6.19$ . The screw head features a hexalobe head as per ISO 10664 for optimal torque transmission. Since the mandible is not an easily accessible region, the system allows up to 15 deg of angular insertion. Finite element analysis was performed to optimize the dimensions of the plate. The final dimensions corresponded to the results from a comparison of a Ti plate model to the ZX10 plate model in a 4-point bending set up. The goal achieved is a condition of loading at 55 N when the Ti model fails and the ZX10 model does not yet. The model was validated analytically and experimentally. 4-point bending tests conducted on non degraded ZX10 plates measured  $\approx 60$  N of yield load and the Ti plate recorded 28.6 N. The ZX10 plates degraded in simulated body fluid over 8 weeks presented a loss of mechanical strength down to  $\approx 15$  N of yield load. From this, the degradation rate by mass loss was calculated as 1.08 mm/year.

For the cytotoxicity assays, discs of 8 mm diameter and 2 mm thickness were manufactured, polished, predegraded and gamma sterilized. *In vitro* cytotoxicity tests were performed using human dermal fibroblasts in three different assays, indirect contact, direct contact and direct seeding assays. In the indirect contact assay, the effect of degradation products as extracts was tested on cells to assess viability and proliferation, using phase contrast microscopy, LIVE/DEAD® staining and DNA extraction using PicoGreen®. On the third day of culture, the qualitative results showed severe cytotoxicity for 100 % extracts, moderate for 50 % extracts and low for 10 % extracts. These results are comparable to the results in the literature under similar experimental conditions. *In vitro* simulated environments are known to be much harsher than *in vivo*, with no flow to carry away degradation products or pH buffer. In this sense, the results can be considered promising. The direct contact assay tests the reaction of cells when the implant is placed on a confluent cell layer. The results showed living cells in the presence of implants degraded by culture media. The direct seeding assay, where cells were seeded directly on the implant surface, showed no attached and viable cells due to the active surface and hydrogen gas release. All tests were performed in accordance with ISO 10993-5.

ZX10 with relatively uniform and low corrosion rates shows tremendous potential in fracture fixation as screw plate systems. The biocompatibility of the naturally occurring elements in the alloy

provides confidence over other Mg alloying systems which contain rare earth elements. The initial findings from the first implant prototype are promising for use in the mandible. More biomechanical oriented tests and *in vitro* assays will provide a better understanding of the material and the reactions of cells to the material, optimize dimensions and help with further material development.

With a yield strength up to 280 MPa and other properties close to those of bone (Young's modulus  $\approx 20$  GPa and density  $1.1\text{ g/cm}^3$ ), such as Young's modulus of 45 GPa and density of  $1.738\text{ g/cm}^3$ , the material can bring about a paradigm shift in craniomaxillofacial fracture fixation.





# Contents

<b>List of Figures</b>	<b>xiii</b>
<b>List of Tables</b>	<b>xvii</b>
<b>1 Introduction</b>	<b>1</b>
1.1 Background . . . . .	1
1.2 Biodegradable materials in fracture fixation . . . . .	1
1.2.1 Mg-Zn-Ca alloy - ZX10 . . . . .	3
1.3 Mandibular angle fractures . . . . .	4
1.3.1 State of the art in mandibular angle fixation . . . . .	4
1.4 Motivation and hypothesis of the thesis . . . . .	5
1.4.1 Workflow . . . . .	5
<b>2 Material and methods</b>	<b>7</b>
2.1 Sample material selection . . . . .	7
2.1.1 Raw material . . . . .	7
2.1.2 Material characterization . . . . .	7
2.1.3 Observations . . . . .	9
2.1.4 Sample material selection result. . . . .	12
2.2 Implant designing . . . . .	12
2.2.1 Screws . . . . .	12
2.2.2 Plates . . . . .	13
2.2.3 FE Model . . . . .	13
2.3 Mechanical testing . . . . .	14
2.3.1 Pull out test . . . . .	14
2.3.2 Degradation by immersion in simulated body fluid . . . . .	15
2.3.3 4-point bending test . . . . .	17
2.4 <i>In vitro</i> testing . . . . .	19
2.4.1 Sample preparation . . . . .	19
2.4.2 Cell bank preparation . . . . .	20
2.4.3 Indirect contact assay . . . . .	21
2.4.4 Direct contact assay . . . . .	22
2.4.5 Direct seeding assay . . . . .	22

<b>3</b>	<b>Results</b>	<b>25</b>
3.1	Implant designing . . . . .	25
3.1.1	FE analysis . . . . .	25
3.1.2	Final design of the implants . . . . .	25
3.2	Mechanical testing . . . . .	28
3.2.1	Pull out tests . . . . .	28
3.2.2	4-Point bending. . . . .	29
3.2.3	Degradation by immersion in SBF . . . . .	32
3.3	<i>In vitro</i> tests . . . . .	34
3.3.1	Indirect contact assay . . . . .	34
3.3.2	Direct contact assay . . . . .	37
3.3.3	Direct seeding assay . . . . .	40
<b>4</b>	<b>Discussion</b>	<b>43</b>
4.1	Mechanical tests . . . . .	43
4.1.1	Pull out test . . . . .	43
4.1.2	4 point bending test . . . . .	44
4.1.3	Degradation in SBF. . . . .	45
4.2	Implant designing . . . . .	45
4.3	<i>In vitro</i> tests . . . . .	46
4.3.1	Indirect contact assay . . . . .	46
4.3.2	Direct contact assay . . . . .	47
4.3.3	Direct seeding assay . . . . .	48
4.3.4	Overall. . . . .	48
<b>5</b>	<b>Recommendations for future work</b>	<b>51</b>
<b>6</b>	<b>Conclusion</b>	<b>53</b>
<b>A</b>	<b>Raw material analysis</b>	<b>55</b>
A.1	Fraction of recrystallization . . . . .	55
<b>B</b>	<b>CAD drawings</b>	<b>59</b>
<b>C</b>	<b><i>In vitro</i> detailed results</b>	<b>63</b>
	<b>Bibliography</b>	<b>67</b>

# List of Figures

1.1	Difference in degradation rate of ZX50 with extra high pure Mg and commercially pure Mg as reported in Hofstetter et al [1]. . . . .	3
1.2	Image depicts a mandibular angle fracture fixed by a miniplate system. Image is a copyright of the AO foundation [2] . . . . .	4
1.3	Illustration represents various tools that were used to biomedically characterize ZX10 for fracture fixation. . . . .	5
2.1	Different planes of observations for the extruded plate (A-A), screw and disc (C-C) raw material. . . . .	8
2.2	Grain size estimation by linear intercept method as seen on the KEYENCE microscope. . . . .	9
2.3	Front end of the extruded raw material to manufacture screws corresponding to batch A12-CO2-R1-S3. Sub figure (a) is representative of the microstructure of the sample at a low magnification and sub figure (b) is a magnified region from where grain size could be estimated. . . . .	10
2.4	Rear end of the extruded raw material to manufacture screws corresponding to batch A12-CO2-R5-S1. Sub figure (a) is representative of the microstructure of the sample at a low magnification and sub figure (b) is a magnified region from where grain size could be estimated. . . . .	10
2.5	Front end of the extruded raw material to manufacture plates corresponding to batch A12-CO3-R1. Sub figure (a) is representative of the microstructure of the sample at a low magnification and sub figure (b) is a magnified region from where grain size could be estimated. . . . .	11
2.6	Rear end of the extruded raw material to manufacture plates corresponding to batch A12-CO3-R6. Sub figure (a) is representative of the microstructure of the sample at a low magnification and sub figure (b) is a magnified region from where grain size could be estimated. . . . .	11
2.7	The extruded raw material to manufacture discs corresponding to batch A12-C01. Sub figure (a) is representative of the microstructure of the sample at a low magnification and sub figure (b) is a magnified region from where grain size could be estimated. . . . .	12
2.8	First prototype of screws (a) and plates (b). Figures not to scale. . . . .	13
2.9	Load and boundary conditions applied for Ti (top) and ZX10 (bottom) plate in the FE model, to optimize the dimensions of the ZX10 plate. . . . .	14

2.10 DePuy Synthes Ti screw and in house manufactured ZX10 screw used in the pull out experiment. Length of the screw and outer diameter are indicated. . . . .	15
2.11 Experimental set up of the pull out tests showing the Ti screw inserted in artificial bone, held by the hook with a spherical recess. The artificial bone is clamped and a constant grip span is maintained between the clamps. . . . .	16
2.12 A SBF degraded implant disc after removal of water soluble salts. . . . .	17
2.13 Degradation set up of the plate samples showing the CO <sub>2</sub> buffering system and how the plates were confined. The black box indicates samples of batch A12-C03-R2 and all other samples were from batch A12-C03-R3. . . . .	18
2.14 Experimental set up for the 4-point bending experiment showing a ZX10 sample placed symmetrically between the upper and lower supports. . . . .	19
2.15 Discs manufactured for in vitro tests. Sub-figure (a) represents the machined surface and sub-figure (b) represents a P4000 grit polished surface. . . . .	20
2.16 Indirect contact experiment plan with a representation of the culture plate. One plate was prepared per time point. . . . .	22
2.17 Direct contact experiment plan showing implant placement on a confluent cell layer.	23
2.18 Direct seeding experiment plan showing cells cultured on top of the implant surface.	23
3.1 Von Mises stress patterns obtained for ZX10 plate and the Ti plate for a load case of 55 N. Top and bottom indicate the stress on the respective surface of the plate where the load and constraints were applied. . . . .	26
3.2 The displacement observed for a load case off 55 N for the ZX10 plate and the Ti plate. Images represent the actual representation x 0.5. . . . .	26
3.3 Final design of the screw (a) and plate (b). Figures not to scale. . . . .	27
3.4 Assembly of the screw plate system showing orthogonal screw and screw inserted at 15°. . . . .	27
3.5 A typical pull out graph showing load in N vs displacement in mm for a ZX10 screw. .	28
3.6 Pull out strength recorded for Ti and ZX10 screws, normalized to insertion depth of threaded length. The value represents the mean of N samples and error bars represent standard deviation. . . . .	29
3.7 ZX10 screw after pull out testing as observed by high resolution microscopy. The screw head was not manufactured as it was not required for the test. Subfigure (a) shows the whole screw and Subfigure (b) shows a magnified view which confirms there was no shearing of the screw threads. . . . .	29
3.8 The figure shows a ZX10 sample that underwent loading and bent in a ductile manner. All tested samples showed similar behaviour. . . . .	30
3.9 A typical 4 point bending graph showing load in N vs displacement in mm for a ZX10 plate (Green). The yield load (red) was estimated by calculating the slope (blue), drawing a line having an offset of 0.02 mm (yellow) from the slope and checking the intercept.	30

- 3.10 Graph represents the yield load in 4 point bending tests for 2 samples of each batch. Non degraded samples and samples degraded in SBF were tested after every week, upto 4 weeks for batch A12-C03-R2 and upto 8 weeks for batch A12-C03-R3. . . . . 32
- 3.11 Degradation rates recorded for each sample after every week of degradation upto 8 weeks in SBF. The corrosion rate for each sample is calculated for the whole period of degradation up until that point. R2 represents batch A12-C03-R2 and R3 represents batch A12-C03-R3. The symbols '\*' and '#' denote the discrepancies in temperature and pH noted in the set up, respectively, due to equipment malfunction as elaborated in previous sections. . . . . 34
- 3.12 Cell proliferation and viability recorded by DNA quantification using Quant-iT™ PicoGreen® for different concentrations of extracts in the indirect contact assay. Results represent the mean of experimental quadruplets and technical triplicates. Error bars represent one standard deviation. Symbol '\*' on D1 time-point represents a significant difference between 0 % and 100 % extract group with  $p = 0.001$  and between 10 % group and 100 % extract group with  $p = 0.007$ . Symbol '\*\*' on D2 time-point represents a significant difference between 0 % and 50% group with a  $p = 0.001$  and between 0 % and 100 % group with  $p = 0.000$ . Symbol '\*\*\*' on D3 time-point represents a difference between all groups. Between 0 % and 10 %, 50 %, 100% groups a  $p = 0.001$ ,  $p = 0.000$  and  $p = 0.000$  was noted, respectively. The 10 % groups showed a significant difference to 50 % and 100% group with  $p = 0.000$ . The 50 % group showed a significant difference to 100 % group with  $p = 0.023$ . . . . . 35
- 3.13 Phase contrast and LIVE/DEAD® assay after day 1 and day 3 of the indirect contact assay. Only the live channels are recorded due to a technical difficulty. Long spindle shaped cells of the phase contrast images indicate healthy cells and green spots from the Live/Dead study indicate live cells. . . . . 36
- 3.14 Direct contact assay culture wells showing change in colour after 3 days (right). ND represents non degraded implants. Control wells contain only cells. . . . . 37
- 3.15 Observation of degradation products in the wells of the direct contact experiment. . . 38
- 3.16 Control wells with no implant discs showing well attached and healthy looking cells in bright-field (a) and fluorescent (b) mode. . . . . 38
- 3.17 Non-degraded implants observed after 72 h on direct contact with cell layer. Sub-figure (a) shows rounded cells and few attached healthy looking cells and sub-figure (b) confirms the same with LIVE/DEAD® stain. Very mild green signal is seen in small spots indicating dying cells. . . . . 39
- 3.18 The edge of the culture well shows well attached healthy looking cells seen in bright field mode in sub- figure (a) and sub-figure (b) shows the same spot using fluorescent mode to visualize the LIVE/DEAD® stain. Live cells are indicated by green and dead cells by red spots. . . . . 39

3.19 SBF degraded implants observed after 72 h on direct contact with cell layer. Sub- figure (a) shows cell debris and no visibly healthy cells and sub figure (b) confirms the same with LIVE/DEAD <sup>®</sup> stain. Very mild green signal is seen in small spots indicating dying cells. . . . .	40
3.20 DMEM degraded implants observed after 72 h on direct contact with cell layer. Sub- figure (a) shows rounded and dying cells near the implant edge and sub figure (b) confirms the same with LIVE/DEAD <sup>®</sup> stain showing many red spots. . . . .	41
3.21 Well attached and healthy looking cells observed under the DMEM degraded implant surface. . . . .	41
3.22 Non degraded implant surface after day 4 of direct seeding assay showing many bubbles indicated by white arrows and red signal of the LIVE/DEAD <sup>®</sup> stain indicating dead cells. . . . .	42

# List of Tables

2.1	Extrusion parameters, alloying elements and impurities in ppm wt. as measured by ICP-OES and GDMS of the raw materials . . . . .	8
2.2	Batch number of samples used for various purposes and the embedding procedure followed. . . . .	8
2.3	Chemical composition and weight of salts added in the given order to 5 L of magnetically stirred deionised water at 37 °C, to prepare simulated body fluid (SBF). . . . .	16
2.4	Leachable preparation at different concentrations for the indirect contact <i>in vitro</i> experiment. . . . .	22
3.1	Table represents force values and corresponding stiffness recorded for non degraded and degraded plate samples of two batches (A12-C03-R2 and A12-C03-R3) in 4 point bending. Value represents the loads at which the material plastically deforms (Yield point) and corresponding stiffness. Two samples were recorded for each condition of each batch. . . . .	31
3.2	Mass losses recorded for two samples of two batches of ZX10 plate samples, over 4 weeks for batch A12-C03-R2 and 8 weeks for batch A12-C03-R3. The samples were degraded in SBF, the corrosion products were removed and then weighed. . . . .	33
3.3	pH recorded after 24 h (Day 1) and 72 h (Day 3) of exposing implant discs to culture media in various concentration. The dilution was performed in fresh media. . . . .	37
4.1	Comparison drawn between parameters in the literature with the thesis which could be a possible explanation to the differences in results observed for cytotoxicity in the indirect contact assay. . . . .	47





# Introduction

## 1.1. Background

Fractures are the most common musculoskeletal trauma's experienced in the orthopedic domain with large socio-economic impacts [3]. Fixation is approached with open and closed reduction techniques, depending on the type of fracture. Various devices are used for open reduction techniques such as pins, screws, plates, nails, external fixators, etc [4, 5]. With advent of better material technology and understanding of orthopedic biology, these methods have proved quite successful. However, these techniques leave an unresolved question in the community, as to whether these devices need to be removed by a second surgery or they are safe to leave inside the body despite having served their purpose [6, 7]. Permanent devices are associated with stress shielding and consequent bone loss effects, necrosis, metallosis, accumulation of wear debris in organs and infections [7]. While surgeons and researchers have varied opinions on this matter in asymptomatic patients, most agree that in pediatric patients these permanent implants hinder skeletal growth and must be removed after fracture healing has been achieved [8, 9]. Irrespective of age, any kind of invasive surgery is taxing on the body and the advantages of avoiding it are abundant. It was with these ideas in mind that biodegradable materials started gaining experimental verification and patents as early as 1960's [10]. However, it was not until recently that a few degradable devices gained market approval as commercial devices [11]. Yet, these are not as popular as the gold standard devices made out of titanium and its alloys due to various complications associated with biodegradable devices.

## 1.2. Biodegradable materials in fracture fixation

The failures and problems associated with biodegradable materials provide valuable insights for developing new materials and characterizing them for clinical applications. Some of these materials are elaborated on below along with their individual disadvantages.

- **Polymers:** The most popular and almost synonymous to biodegradable fixation materials are polymers. Polymers such as Polyglycolic acid (PGA) and Poly-*L*-lactide (PLLA) found clinical applications as early as 1985 [12]. These were plagued with adverse inflammatory responses and mechanical failure which ultimately led them to be replaced by a more robust Poly(*L*-lactide-*co*-*DL*-lactide) (PLDLA) system [13]. However, this was also associated with various undesired physiological responses, such as infections, wound dehiscence and implant displacement. These polymers follow an acidic degradation profile which has been associated with an upregulation of osteoclasts and downregulation of osteoblasts. The state of degradation products has also shown an influence on inflammatory response with amorphous products being more favorable than crystalline debris [14].
- **Composites:** Composites are being experimentally tested such as bioresorbable phosphate based glass (PBG) fibres as a composite material with PLLA films, poly( $\epsilon$ -caprolactone)-(PCL) based tricalcium phosphate (TCP) and TCP/Fe composites and some of these are promising. However, polymer based composites still risk inflammatory responses and ceramic based composites are brittle and risk mechanical failure [15].
- **Degradable metals:** Degradable metals have also gained interest such as magnesium, iron and zinc. While zinc is still in experimental stages [16], iron has been deemed to degrade too slowly thus making it unsuitable for fracture fixation unless developed specifically [17]. Mg was identified as surgical material as early as 1878 by Dr. Edward C Huse [18] but was a forgotten material due to its high corrosion rate accompanied with hydrogen gas evolution, following the reaction  $Mg + 2H_2O \rightarrow Mg(OH)_2 + H_2$ . Recently it has been realized that corrosion properties can be controlled to some extent by alloying Mg with other elements and hydrogen evolution is not detrimental when the evolution rate is low. The early alloys tested included AZ31 containing aluminum, that is associated with neurological toxicity [19]. With time it was also possible to increase the purity of magnesium which reduced the corrosion rate further. Implants based on the Mg alloy WE43 has recently gained the CE mark and commercial bone screws and pins are now available [11]. This alloy contains rare earth elements such as Yttrium and Neodymium, the systemic effects of which are disputed.

From polymers to metals the biggest challenge in degradable fixation devices remain the biocompatibility of the degrading products. It is necessary to develop materials that contain only biocompatible materials that degrade without causing adverse tissue irritant responses. For this reason, Mg alloys with naturally occurring elements in the body gained attention. This report will focus on and characterize the Mg-Zn-Ca alloy, ZX10 (1 % Zn and 0.3 % Ca by weight) based on extra high purity Mg.

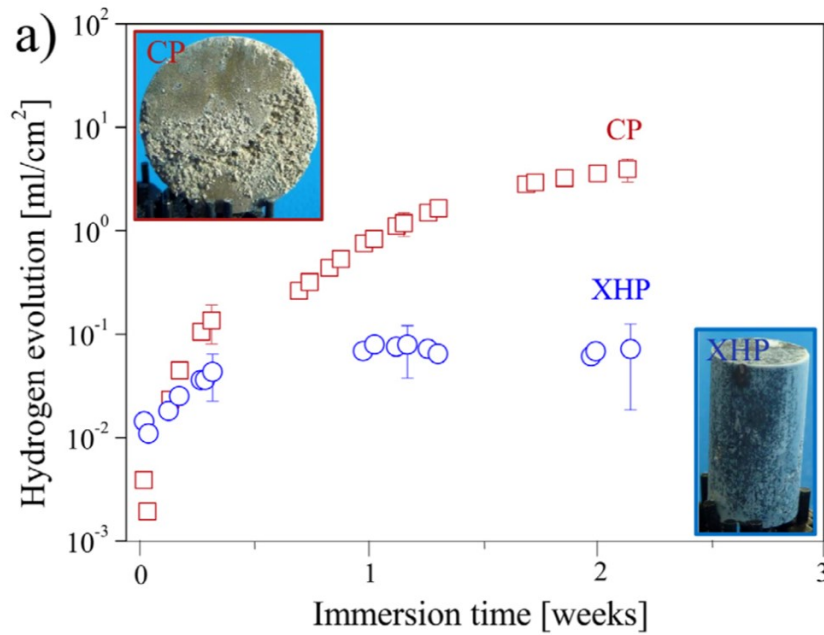


Figure 1.1: Difference in degradation rate of ZX50 with extra high pure Mg and commercially pure Mg as reported in Hofstetter et al [1].

### 1.2.1. Mg-Zn-Ca alloy - ZX10

Mg is an abundant element in the body, most of which is stored in the bone. It is vital in various physiological mechanisms and easily excreted via urine [20]. Mg has a Young's modulus of 45 GPa, close to that of bone at  $\approx 20$  GPa [21, 22], thereby avoiding stress shielding effects as fracture fixators. It has a density of 1.738 g/cm<sup>3</sup> also close to that of mandibular bone at 1.11 g/cm<sup>3</sup> [22, 23] and allows for light weight applications. Ca is naturally occurring in the body, favourable to the bone, has a low density of 1.55 g/cm<sup>3</sup> and has shown to improve corrosion resistance when added to Mg [24]. Zinc is another biocompatible element recognized for its corrosion resistance properties when added to Mg and Ca in less than 2 % by weight [1, 24]. Commercially pure Mg has high and unpredictable corrosion trends associated with the high concentrations of trace impurities, such as Fe, Cu, Ni and Co [1]. To circumvent this problem, ultra high purity (XHP) Mg with purity 99.999% was produced by vacuum distillation [25] with Ca (99.99%) and Zn (99.999%) having the composition 1 weight% Zn and 0.3 weight% Ca, i.e., ZX10. It was hypothesized that this novel alloy would provide the advantages of Mg while drastically reducing corrosion rates based on the results on ZX50 (5 weight% Zn and 0.3 weight% Ca) as seen in Figure 1.1. This lean alloy produced by indirect extrusion where fine grains are formed, has a yield strength up to  $\approx 240$  MPa, tensile strength  $\approx 265$  MPa, elongation to fracture  $\approx 30\%$  and a low mechanical anisotropy of  $\approx 1.15\%$  [26]. In ongoing experiments a yield strength of 280 MPa could be achieved and it is envisioned to improve further by modifications in the manufacturing process. The mechanical properties of the alloy make it suitable for low load bearing applications and for such a case, it has been evaluated in this thesis.

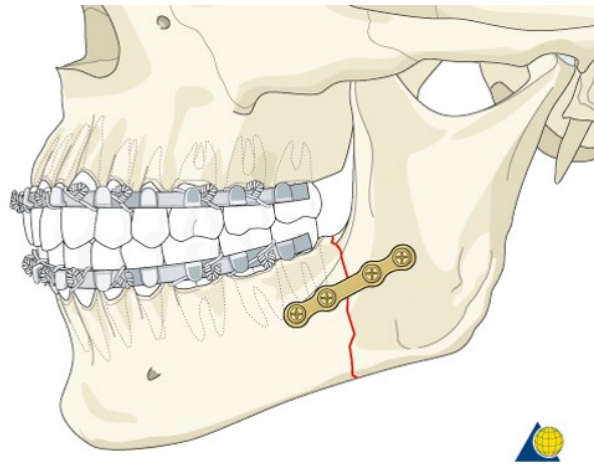


Figure 1.2: Image depicts a mandibular angle fracture fixed by a miniplate system. Image is a copyright of the AO foundation [2]

### 1.3. Mandibular angle fractures

Motor vehicle accidents and assaults account for the highest cause of mandibular fractures. Other causes include falls and gun shot wounds and men appear more prone to this type of trauma [27]. The most common mandibular fractures is reported to be angle fractures, that are most popularly treated by open reduction methods using miniplate systems [27–29]. A typical angle fracture and fixation by a miniplate system is shown in Figure 1.2. Infections, dehiscence and the healing sensitivity associated with this load bearing region lead to increased susceptibility to removal of the implants and therefore second surgery [28, 29]. The ZX10 material is therefore envisioned for application in the treatments of angle fractures. Mg and alloys are speculated to have anti bacterial effects [30] and with the improved strength of ZX10, the material is expected to serve well in this low load bearing region.

#### 1.3.1. State of the art in mandibular angle fixation

The angle of the mandible is subjected to complex forces due to the region being in the abrupt cross-road of horizontal to vertical rami. The presence of the third molar also makes the region behave like a "lever" [31]. Angle fracture fixation is a challenging tasks for surgeons due to the high complication rate associated with infections, malunions, malocclusion and facial nerve damage. Various fixation techniques are available and in Europe, the Champy technique (mini plate on the lateral aspect of mandible) is the most commonly used technique followed by the two plate technique [32]. The 3D plates are another favourite. These plates are resistant to forces in three dimensions, shear, bending and twisting forces. These have shown to perform better than two plate systems when the fracture line is closer to the condyle [33]. Over the years, many techniques have evolved and recently with tools such as finite element (FE) analysis, researchers and surgeons are at a better position to opt for the treatment techniques that are best suited to each patient and their unique fracture. FE

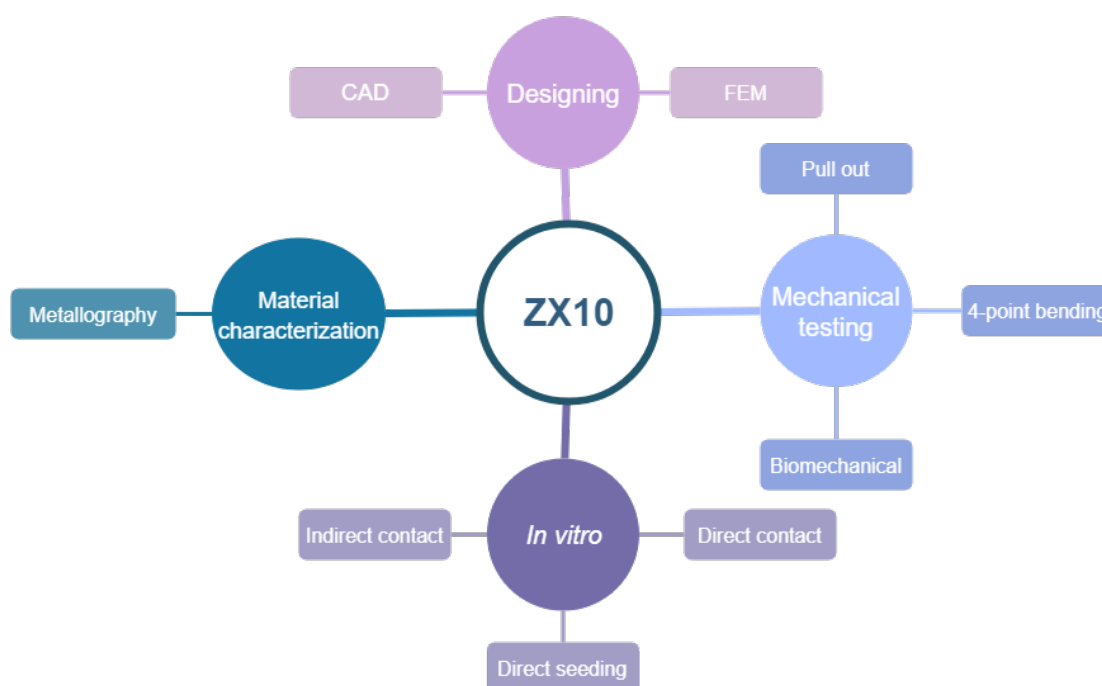


Figure 1.3: Illustration represents various tools that were used to biomedically characterize ZX10 for fracture fixation.

models comparing various fixation techniques as shown in Patussi et al conclude that the Champy technique shows more tension in plate and screws and also more stress on the bone which is not favourable [31]. The study shows locking plates placed in parallel provide more stability and less stresses on the bone as compared to conventional plates placed in the same manner. As of now, the choice of technique seems an imperative of the surgeon.

## 1.4. Motivation and hypothesis of the thesis

The work in this thesis aims to develop application specific implant prototypes and to check the suitability of the ZX10 alloy in terms of mechanical strength and biocompatibility. It is therefore hypothesized that,

- The ZX10 material can be designed as implants of acceptable dimensions to provide mechanical strength comparable to commercially available devices used in the CMF region.
- This material or its degradation products will not exhibit cytotoxic effects *in vitro*.

### 1.4.1. Workflow

To test the hypotheses, the work in the thesis was basically divided into four sections. This is elaborated below and represented in Figure 1.3

- **Material selection:** The first section included analyzing the raw material and understanding the importance of manufacturing parameters and its effects on the microstructure, leading to the selection of appropriate materials for further use.

- Implant designing: Computer aided design (CAD) models of the envisioned implant parts were rendered, optimized using finite element methods (FEM) and sent for manufacturing.
- Mechanical testing: The manufactured parts were mechanically tested in comparison to a commercially available titanium implant of the CMF region. Material was also tested after degradation in simulated body fluid.
- *In vitro* testing: The implant material and its degradation products were tested for cytotoxicity in various cell culture experiments.

All four of the above work sections are deemed equally important to test the feasibility of the ZX10 alloy for applications as a screw plate system to treat mandibular angle fractures. The thesis report will further elaborate on all methods and results, and further discuss the biomedical characterization of the ZX10 alloy.

## Material and methods

### 2.1. Sample material selection

#### 2.1.1. Raw material

The raw material, denominated ZX10 having a nominal composition of 1 wt % Zn and 0.3 wt % Ca, was manufactured by indirect extrusion [26] in three batches for the three envisioned requirements. The extrusion parameters and the elemental composition of the alloy are given in Table 2.1. Here the batch number A12-C01 represents the material used to prepare samples for *in vitro* tests, A12-C02 represents the material used to manufacture screws and A12-C03 represents the material used to manufacture plates. During the manufacturing process of the raw material for screws, a discrepancy in temperature was noted. Towards the end of extrusion the temperature raised from 340 °C to 360 °C. In the case of raw material for plates a change in speed was noted. The speed dropped from 0.2 mm/s to 0.03 mm/s. These changes in parameters may have led to changes in the microstructure of the material, thus requiring to study the material using metallographic techniques. This analysis is further elaborated in the next section.

#### 2.1.2. Material characterization

Microstructural characteristics provide important information regarding the strength, ductility and homogeneity of the material. For this purpose, the sample needs to be embedded, ground on the required plane of observation, etched and then evaluated under an optical microscope. In this research, several samples from different material batches were evaluated. Two samples for the plates and screws, and one sample for the discs were characterized. The sample corresponding to the discs was only undertaken for observation, whereas the samples from plates and screws were evaluated to decide on the final raw material, from which the first prototype of implants would be manufactured. The samples were evaluated in different planes of observation as represented in Figure 2.1.

Batch number	A12-C01	A12-C02	A12-C03
Cross-section	10 mm $\phi$	6 mm $\phi$	9 x 3.5 mm
Extrusion ratio	25	69	79
Temperature	325 °C	340 °C $\rightarrow$ 360 °C	360 °C
Speed	0.2 mm/s	0.03 mm/s	0.2 mm/s $\rightarrow$ 0.03 mm/s
Pulling load	200 N	300 N	300 N
Zn	0.96 wt %	0.96 wt %	0.971 wt %
Ca	0.29 wt %	0.299 wt %	0.34 wt %
Fe	0.54	1.2	0.42
Ni	0.08	0.12	0.08
Co	0.006	0.02	0.02
Cu	0.34	0.89	0.15
Pb	4.6	1.2	5.3

Table 2.1: Extrusion parameters, alloying elements and impurities in ppm wt. as measured by ICP-OES and GDMS of the raw materials

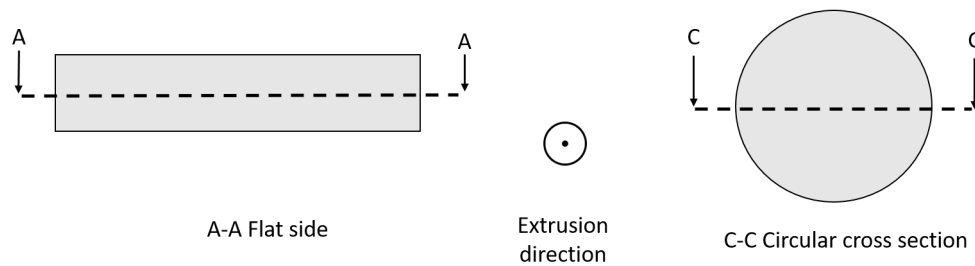


Figure 2.1: Different planes of observations for the extruded plate (A-A), screw and disc (C-C) raw material.

Observation across A–A represents the longitudinal section of a plate. For the screws and discs, the observation plane is C–C. The extrusion direction represented by the symbol is either into or out of the plane. Hot and cold embedding procedures were followed for samples as specified in Table 2.2. In the grinding process, the samples were prepared with a P120 grit SiC paper from Struers, at 30 N load using a Struers Rotopol-1 grinding machine to approach the central plane. The samples then underwent grinding at P500, P2500 and P4000 for a fine finish. These samples were then etched using a picric acid based etchant. The pre-prepared etchant had a composition of 4 g picric acid, 70 ml ethanol, 10 ml acetic acid and 10 ml water. The solution was dabbed in a cotton swab and wiped on the sample surface for 10 s. These samples were then washed with isopropanol, dipped in

Purpose	Sample number	Procedure
Plates	A12-C03-R1	Cold embedded
	A12-C03-R6	
Screws	A12-C02-R1-S3	Hot embedded
	A12-C02-R5-S1	
Discs	A12-C01-R1-S3	

Table 2.2: Batch number of samples used for various purposes and the embedding procedure followed.



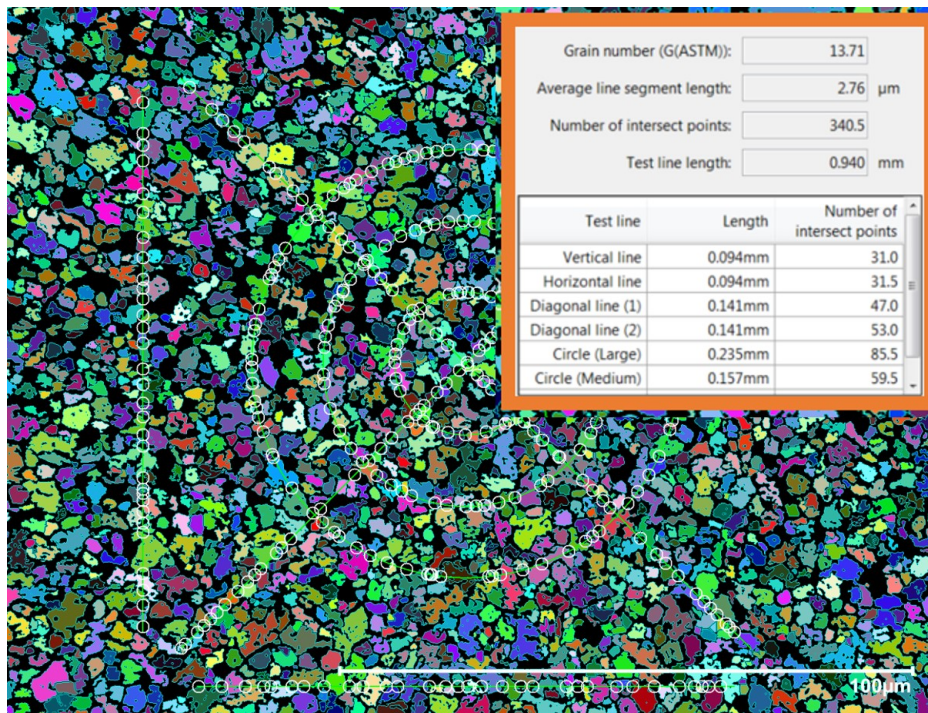


Figure 2.2: Grain size estimation by linear intercept method as seen on the KEYENCE microscope.

the same for rigorous wash and then dried under pressurized air. The samples were then visualized under a Leica DFC450 light microscope at 20x magnification to look for visible grains. Final images were recorded on a KEYENCE VHX-7000 series microscope. The mean grain size was estimated by an automated tool of the microscope using the linear intercept method. An example is shown in Figure 2.2. The importance of quantifying the volume fraction of recrystallization to estimate strength and ductility is well elaborated in J.Hofstetter et al [34]. The fraction of recrystallization, denoted by  $V^{RX}$  was estimated in this work by using basic image processing tools such as binarisation and despeckling of noise, removing outliers, eroding and dilating the image on ImageJ. Comparisons were drawn visually to the original microstructure image and then the  $V^{RX}$  % was estimated from the histogram. Side by side comparisons of the image processing are given in Appendix A.1.

### 2.1.3. Observations

#### Raw material for screws

During the extrusion process, some variability in parameters was noted. The beginning of the extrusion noted a temperature of 340 °C which increased to 360 °C by the end of the extrusion. The extrusion speed also increased towards the end of the rod. These changes led to the different microstructural characteristics depicted in Figure 2.3 and Figure 2.4. The sample from the front end of the rod corresponding Figure 2.3, sub-part (a) showed large areas of non-recrystallized grains, the  $V^{RX}$  was determined to be 51.58 %. The details are elaborated in Appendix A.1. A higher magnification is shown in sub- part (b) from which a mean grain size of 2.24  $\mu\text{m}$  was determined by automated calculation from the microscope. The sample from the end of the rod corresponding to

sub- part (a) of Figure 2.4 showed few areas of non recrystallized grains, the  $V^{RX}$  was determined to be 91.7 %. From a higher magnification depicted in sub-part (b), a mean grain size of  $2.76 \mu\text{m}$  was recorded.

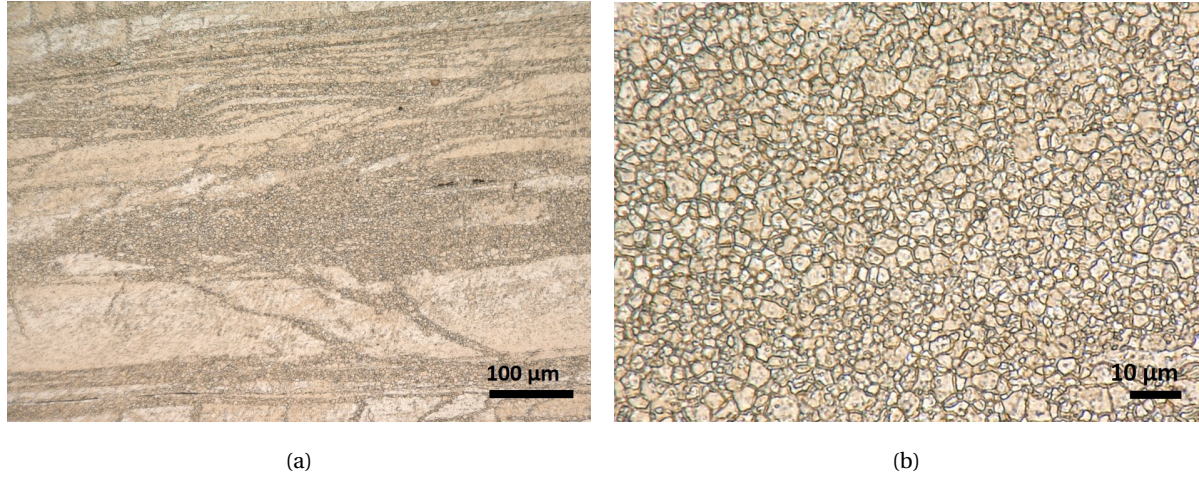


Figure 2.3: Front end of the extruded raw material to manufacture screws corresponding to batch A12-CO2-R1-S3. Sub figure (a) is representative of the microstructure of the sample at a low magnification and sub figure (b) is a magnified region from where grain size could be estimated.

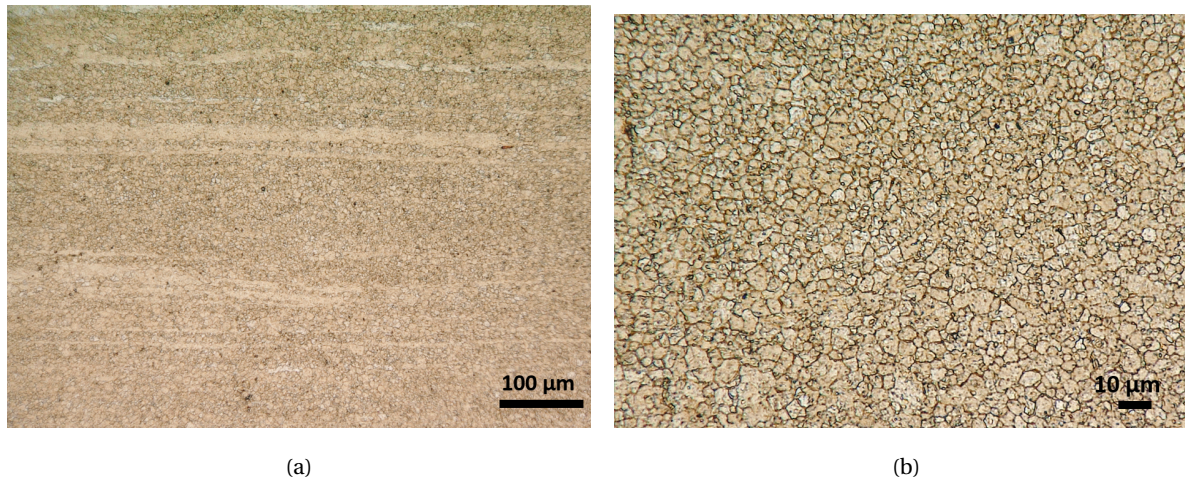


Figure 2.4: Rear end of the extruded raw material to manufacture screws corresponding to batch A12-CO2-R5-S1. Sub figure (a) is representative of the microstructure of the sample at a low magnification and sub figure (b) is a magnified region from where grain size could be estimated.



### Raw material for plates

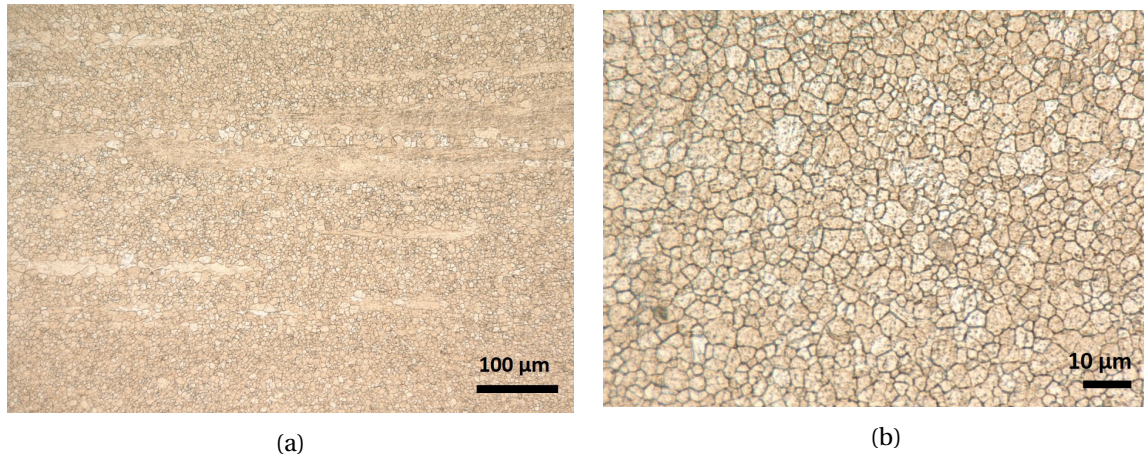


Figure 2.5: Front end of the extruded raw material to manufacture plates corresponding to batch A12-C03-R1. Sub figure (a) is representative of the microstructure of the sample at a low magnification and sub figure (b) is a magnified region from where grain size could be estimated.

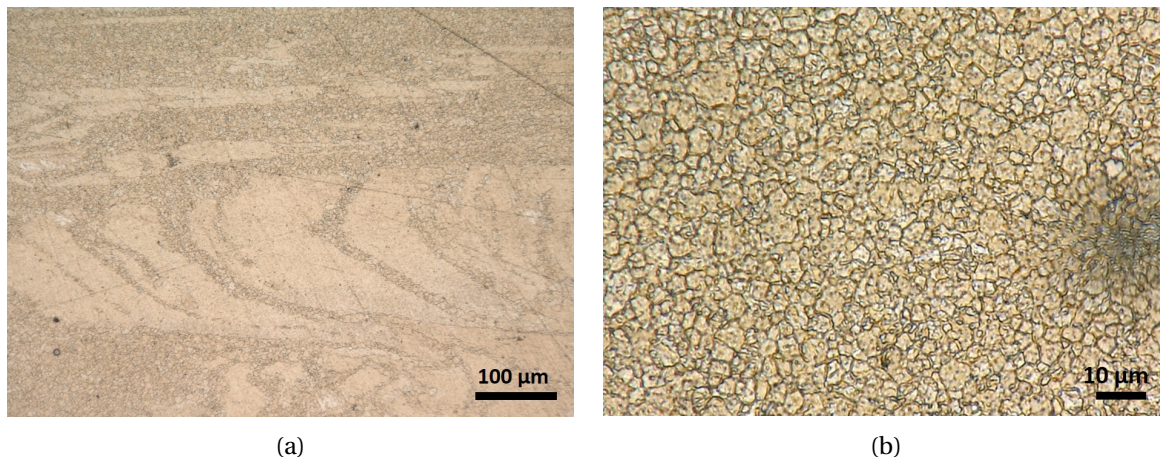


Figure 2.6: Rear end of the extruded raw material to manufacture plates corresponding to batch A12-C03-R6. Sub figure (a) is representative of the microstructure of the sample at a low magnification and sub figure (b) is a magnified region from where grain size could be estimated.

The longitudinal side of the samples from the front and rear end of the extruded bar was chosen for analysis. During the extrusion process for the plate samples, the temperature remained constant at 360 °C however, the extrusion speed dropped towards the end of the bar. This change of speed could lead to the different microstructural characteristics depicted in Figure 2.5 and Figure 2.6. The sample from the front end of the rod corresponding Figure 2.5, sub-part (a) showed few areas of non recrystallized grains,  $V^{RX}$  was determined to be 89.87 %. The details are elaborated in Appendix A.1. A higher magnification image is shown in sub- part (b), from which a mean grain size of 2.88 μm was noted by automated calculation from the microscope. The sample from the rear end of the rod corresponding to sub- part (a) of Figure 2.6 showed large areas of non recrystallized grains, the  $V^{RX}$  was determined to be 53.4 %. From a higher magnification image depicted in sub-part (b), a mean

grain size of  $2.15\ \mu\text{m}$  was recorded. The dark spot in this figure is an artifact of the lens.

#### 2.1.4. Sample material selection result

From the above methods, sample material selection was performed for screws and plates. The raw material corresponding to batch number A12-C02-R5 which was the rear end of the extruded rod was chosen for manufacturing screws and the raw material corresponding to batch number A12-C03-R1 which was the beginning of the extruded bar was chosen for manufacturing plates. In both cases, the material with a higher  $V^{\text{RX}}$  was chosen in order to not compromise on ductility of the materials [26].

#### Raw material for discs

The metallography of the raw material for disc was performed to gain insight about the material but there was no choice of material made for the discs. Figure 2.7, sub-part (a) shows areas of non-recrystallized grains. A higher magnification is shown in sub- part (b) from which a mean grain size of  $2.88\ \mu\text{m}$  was determined by automated calculation from the microscope.

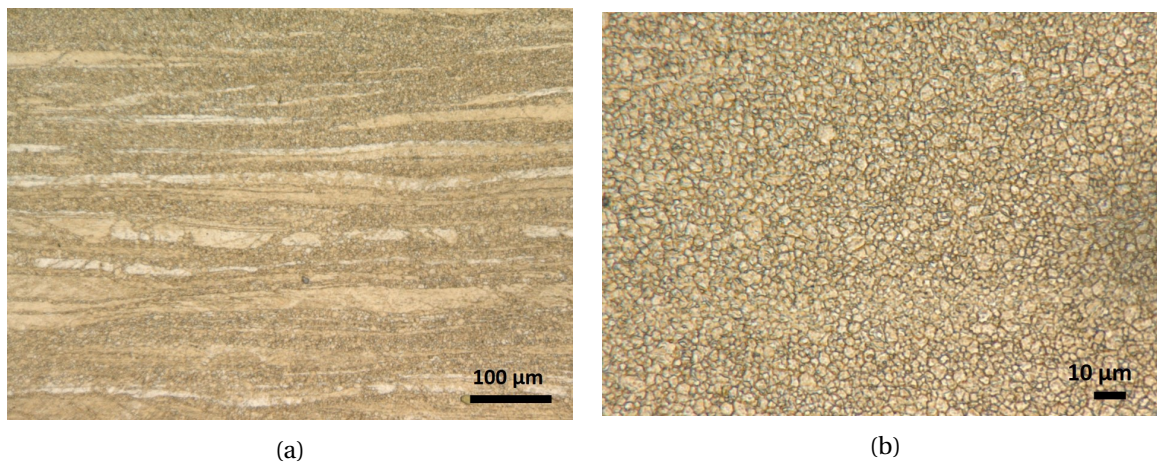


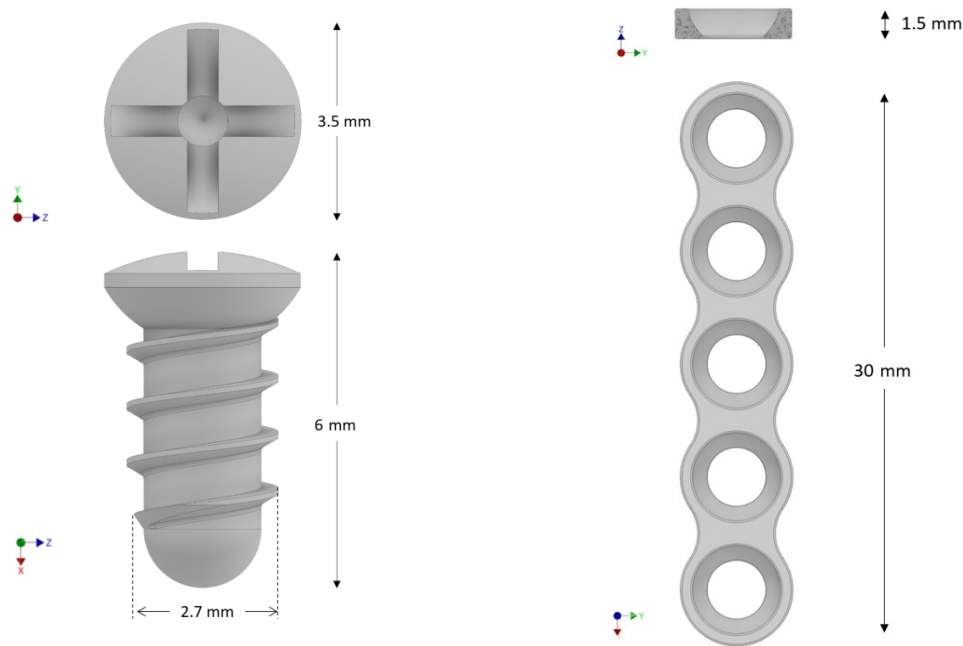
Figure 2.7: The extruded raw material to manufacture discs corresponding to batch A12-C01. Sub figure (a) is representative of the microstructure of the sample at a low magnification and sub figure (b) is a magnified region from where grain size could be estimated.

## 2.2. Implant designing

The Plates and screws were designed based on existing systems in terms of basic dimensioning. Autodesk® Inventor® Professional 2018 software was used to model both plates and screws.

### 2.2.1. Screws

The goal defined for the first prototype was to achieve a pull out strength comparable to that of the Ti systems used in the CMF region. The target was achieved by adjusting structural properties of the screw, such as the outer diameter. Since Ti is stronger than Mg, a Mg screw with a larger outer diameter was envisioned to achieve a comparable pull out strength to the Ti screws. The pull out



(a) Top and front view of the first manufactured screws (b) Top and front view of the first prototype design of the ZX10 plate that were used in the pull out tests.

Figure 2.8: First prototype of screws (a) and plates (b). Figures not to scale.

strength is estimated to be linearly proportional to the outer diameter of the screw and therefore this parameter was chosen to be varied. The first prototype manufactured is shown in Figure 2.8a. This manufactured screw was used for pull out experiments, elaborated in further sections.

### 2.2.2. Plates

The design of the plates was made as per suggestions of Dr. Benoit Schaller, an orthopedic surgeon specializing in the CMF region and a collaborator of the project. The number of holes being 5 and an allowance of 1.5 times the thickness of commercial plates were suggested by him. This first prototype, subjected to further design optimization is shown in Figure 2.8b. Since the mandible is not an easily accessible region, the plates were designed to accommodate a 15 degree angular insertion of the screw. The final dimensions were optimized by using finite element (FE) analysis, as elaborated in the following section.

### 2.2.3. FE Model

The FE analysis was performed on the Autodesk® Inventor® Professional 2018 software. The goal of the FE simulation was to optimize the dimensions of the plate by simulating a 4 point bending load case, for which a Ti plate just fails, but a Mg plate does not. The 4 point bending simulation was chosen since it can be verified experimentally. Due to the limitations of the software, the model had to be adapted to apply loads and boundary conditions. Protrusions of 0.1 mm width and 0.01 mm thickness were made on the regions required for constraining and load application, as shown



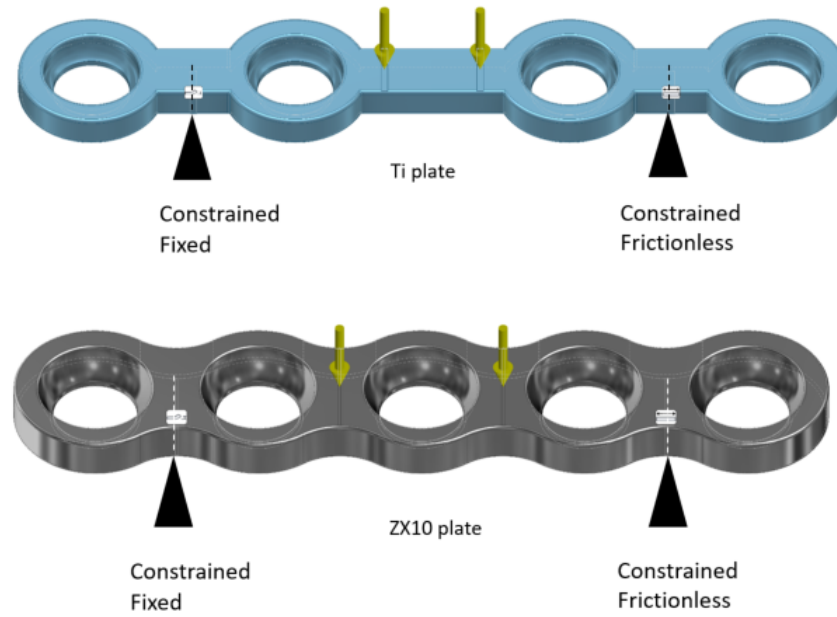


Figure 2.9: Load and boundary conditions applied for Ti (top) and ZX10 (bottom) plate in the FE model, to optimize the dimensions of the ZX10 plate.

in Figure 2.9. The effects of these regions on FE results were checked by modelling the same on a rectangular beam, where analytical solutions for stress and deflection under load exist by employing beam theory and the effects of the protrusions were seen to be negligible. Titanium was modelled as a grade 3 titanium. This is commercially pure Ti with a Young's modulus of 105 GPa and a tensile yield strength of 380 MPa [35]. The plate was estimated to be Grade 3 Ti as a compromise between the popular grade 2 for low load bearing applications such as dental implants and Grade 5 that are used in high load bearing applications such as joint replacements [36]. The higher yield strength of Grade 3 as compared to Grade 2, allowed a safety measure. The ZX10 model was modelled with a Young's modulus of 45 GPa, tensile yield strength of 280 MPa. The ZX10 plate was meshed with 19915 tetrahedral mesh elements and the Ti plate with 10772 tetrahedral mesh elements. In both cases, mesh convergence was observed and accounted for and the analysis was based on linear elastic mechanics only.

## 2.3. Mechanical testing

### 2.3.1. Pull out test

This test was designed to measure the pull out strength of the first prototype of the ZX10 screw and to compare it against a commercially used Titanium bone screw from DePuy Synthes, that is used in the CMF region. The experiment was planned as per suggestions in ASTM F543-17. The screws manufactured in-house did not have a fully formed screw drive at the time of the tests, but just a solid head which was sufficient to grip with a T-handle. Both screws with length and outer diameter dimensions are illustrated in Figure 2.10. Hooks with spherical recesses were manufactured



Figure 2.10: DePuy Synthes Ti screw and in house manufactured ZX10 screw used in the pull out experiment. Length of the screw and outer diameter are indicated.

in-house with a 2.8 mm opening for the Mg screw and 2.1 mm opening for the Ti screw. In both cases the opening was 1 mm more than the outer diameter of the screw. A grip span, indicated between the two clamps was maintained at 3 cm all times. Artificial bone conforming to ASTM F1839 of 40 pcf density from SAWBONES<sup>®</sup> measuring 40 mm thickness was used as the test block. The 40 pcf ( $0.64 \text{ g/cm}^3$ ) block corresponds to density of bone in the maxilla ( $0.67 \text{ g/cm}^3$ ) but not the mandible ( $1.18 \text{ g/cm}^3$ ) [22]. This bone density was still chosen to perform the experiment to be able to compare the results to Kozakiewicz et al, who performed pull out experiments on commercially available maxillofacial screws from the leading manufacturers, DePuy Synthes, Medartis and KLS Martin [37]. Artificial bone also helps to standardize the process and compare results. Holes were predrilled with a 2.2 drill bit for the Mg screw and a 1.8 mm drill bit for the Ti screw as suggested by the surgical manual. The insertion of the screws was done manually. The nominal insertion depth was  $\approx 4.4 \text{ mm}$  measured from the tip of the screw, however this was accurately accounted for while calculating results for each specimen. The pull out rate was set at 1 mm/min. The experimental set up is visualized in Figure 2.11.

### 2.3.2. Degradation by immersion in simulated body fluid

Degradation in simulated body fluid (SBF) was chosen to be determined for two reasons, i) to account for the loss of mechanical strength in the plate samples when they would be further tested

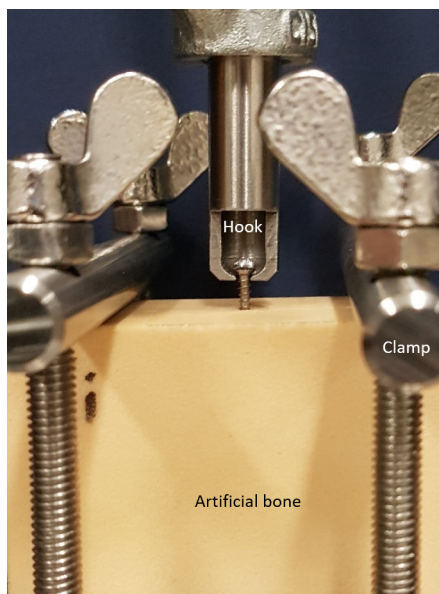


Figure 2.11: Experimental set up of the pull out tests showing the Ti screw inserted in artificial bone, held by the hook with a spherical recess. The artificial bone is clamped and a constant grip span is maintained between the clamps.

Salt	Weight (g)
KCl	1.491
NaCl	29.22
NaHCO <sub>3</sub>	11.3425
Mg <sub>2</sub> SO <sub>4</sub> ·7H <sub>2</sub> O	1.2325
CaCl <sub>2</sub> ·2H <sub>2</sub> O	1.8375
KH <sub>2</sub> PO <sub>4</sub>	0.6805

Table 2.3: Chemical composition and weight of salts added in the given order to 5 L of magnetically stirred deionised water at 37 °C, to prepare simulated body fluid (SBF).

by 4 point bending and ii) to check the effects of a pre-degraded sample in *in vitro* assays. Since the group has established protocols for the experimental set up and SBF formulation [25, 38], the same composition was used to maintain consistency. All glassware and set up used was cleaned with HNO<sub>3</sub> and wiped with alcohol prior to use. The composition of the salts in 5 L of deionised water (dH<sub>2</sub>O) is as given in Table 2.3. The salts were added in the order specified in the table. Only after complete visible dissolution of the added salt was the next salt added. The pH was maintained at 7.41 using a CO<sub>2</sub> buffering system. The pH sensor was placed near the edge of the glass chamber, in close vicinity but without disturbance to the samples. The set up was maintained at 37°C and stirred using a magnetic stirrer at 50-100 RPM to ensure CO<sub>2</sub> dissolution. This degradation method was used twice in the framework of this thesis, once for disc samples and once for plate samples. Details of these are elaborated below.

- Disc: A 2.5 L composition of SBF was used to degrade 30 implant discs for 1 week. The surface area to volume ratio of the disc was 1.5 mm<sup>-1</sup>. No refreshment of the SBF solution was required.



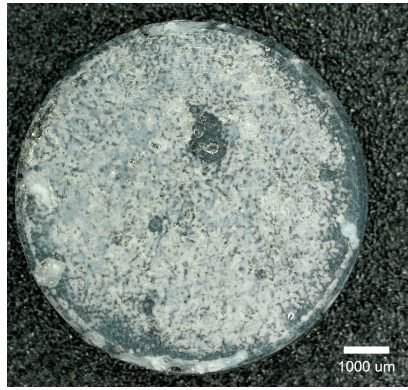


Figure 2.12: A SBF degraded implant disc after removal of water soluble salts.

in this time frame. The samples in total weighed 5.4085 g before immersion and 5.6105 g after immersion due to salt deposition. These samples were left to dry overnight. These were then washed in still dH<sub>2</sub>O for 3 min and subjected to pipette wash of dH<sub>2</sub>O for 1 min, three times to remove the water soluble salts. A washed degraded sample is shown in Figure 2.12. These discs were used in *in vitro* tests, elaborated in further sections.

- **Plates:** A 5 L set up was used to degrade 24 plates over 7 weeks. The surface area to volume ratio of the plate was 2.5 mm<sup>-1</sup>. In this case, the solution was refreshed with dH<sub>2</sub>O after 20 days to compensate for loss by evaporation. The plates were fastened to a plastic plate using sample holders and teflon bands or tie connectors as shown in Figure 2.13. Two batches were evaluated in this set up indicated by the black box. The samples in the black box were from batch A12-C03-R2 and the rest of the samples belonged to batch A12-C03-R3. No difference was expected between these as they were from the same manufacturing batch and from adjacent parts of the extruded bar, yet care was taken to differentiate between these all times. Due to equipment malfunction some discrepancies were noted. After 2 weeks and 6 days, the temperature in the morning was noted as 27 °C which was corrected, however in the evening it went up to 53 °C which was then corrected again and a new temperature sensor was set up. On week 3 day 6, the pH was recorded as 6.75 which was low and CO<sub>2</sub> was continuously being pumped due to a valve malfunction. The valve was then replaced and pH was allowed to raise to 7.41.

### 2.3.3. 4-point bending test

The test was designed to measure the loss of bending strength of plates, from the manufactured plates, to plates degraded in SBF over 8 weeks with a time point at the end of each week of degradation. The test was also used to validate the FE model and to compare the ZX10 plate to a commercially available Titanium plate that is typically used in the CMF region. The set up is shown in Figure 2.14 for a ZX10 sample. A lower span of 18 mm was maintained between the lower supports and the force was applied with an upper span of 6 mm. For the Ti plate an upper span of 3 mm was

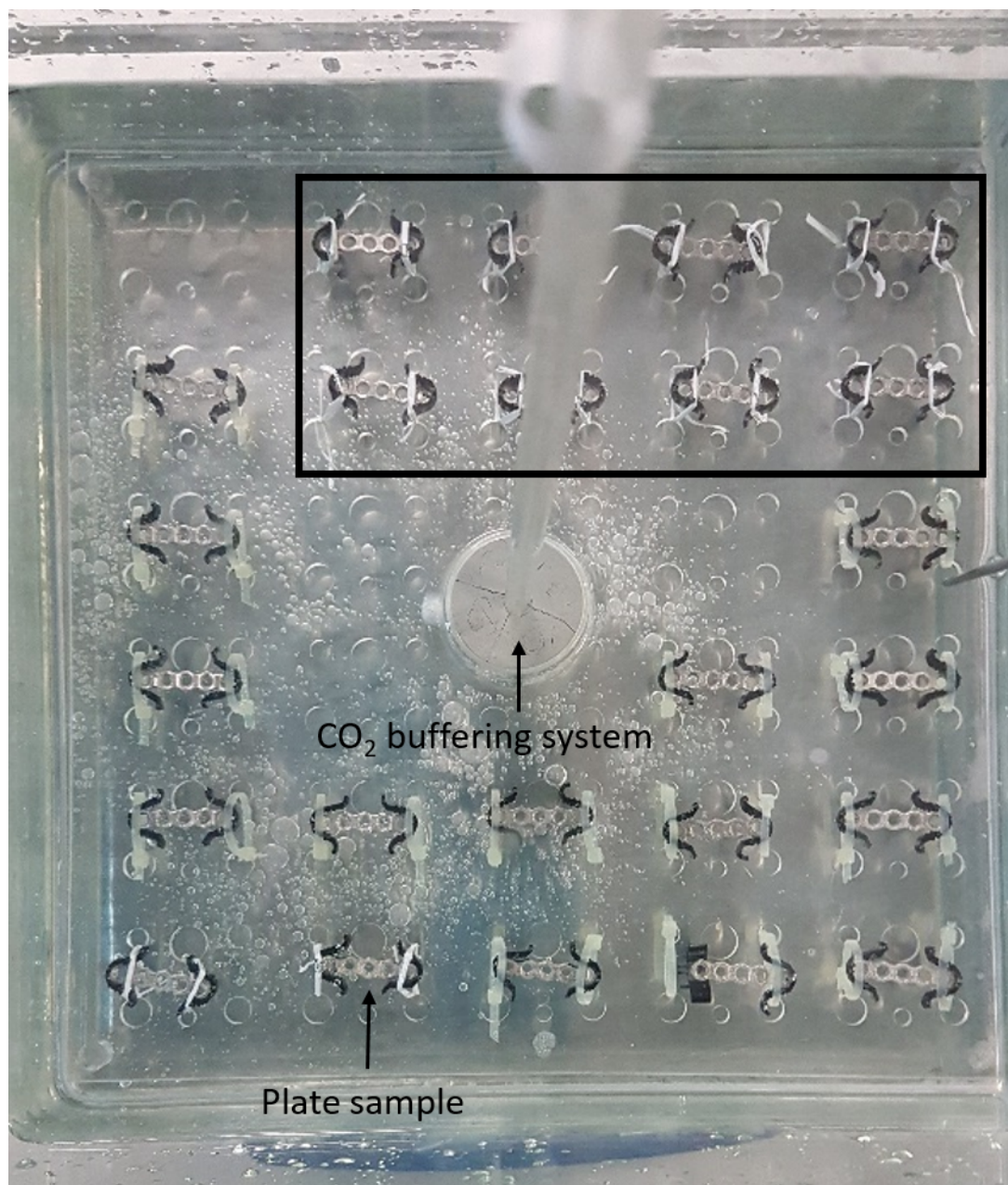


Figure 2.13: Degradation set up of the plate samples showing the CO<sub>2</sub> buffering system and how the plates were confined. The black box indicates samples of batch A12-C03-R2 and all other samples were from batch A12-C03-R3.

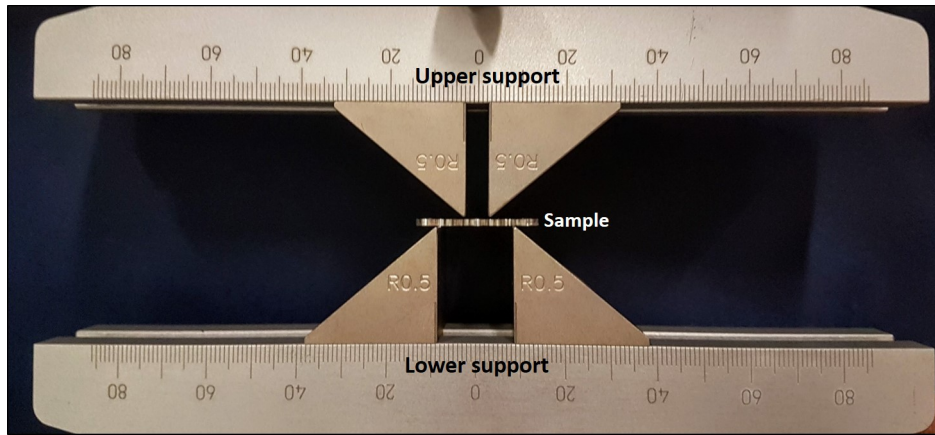


Figure 2.14: Experimental set up for the 4-point bending experiment showing a ZX10 sample placed symmetrically between the upper and lower supports.

maintained and 15 mm for the lower span. The samples were placed symmetrically and loading in compression was allowed in the INSTRON<sup>®</sup> uni-axial testing machine. The ISO 9585 recommendations were attempted but the sample could not be placed in one of the ways suggested and therefore was placed symmetrically. Two samples were tested for each test condition. Once the test was completed, the data was processed on Microsoft<sup>®</sup> Excel 2016. The plots for each sample were generated and a line parallel to the slope of the linear region of the graph was generated at a 0.02 mm offset to reasonably determine the yield load. This was also visually inspected and in some cases the offset was adjusted to 0.015 mm to ensure remaining in the linear region. Post 4 point bending experiments, samples up to 5 weeks of degradation were immersed in  $CrO_3 + AgNO_3$  solution for 1 min to remove the salt deposits from the degradation in SBF. Samples from week 6 to week 8 of degradation were immersed in  $CrO_3 + AgNO_3 + Ba(NO_3)_2$  solution for 1 min for the same purpose. The liquid was changed because the previous solution was no longer strong enough to remove the corrosion products. The samples were then cleaned with ethanol and weighed to measure mass loss and degradation rate.

## 2.4. *In vitro* testing

*In vitro* tests are the first point of biological testing, which can establish potential cytotoxicity, assess morphological changes and give information regarding cell attachment to the implant surface. To that end, three kinds of tests are outlined in further subsections. Before the start of these experiments, the samples were manufactured and treated as per requirement and a cell bank was prepared. Further subsections will elaborate on these methods.

### 2.4.1. Sample preparation

The Mg-Zn-Ca alloy was hot extruded (Batch no. A12-C01). This rod was machined to discs of 8 mm in diameter and 2 mm in thickness. A KERN CD480 turning machine with a WALTER DCGT11T302FS-1 WDN10 tool was used for the production of the discs. Machining was done at 2500 RPM and 0.05



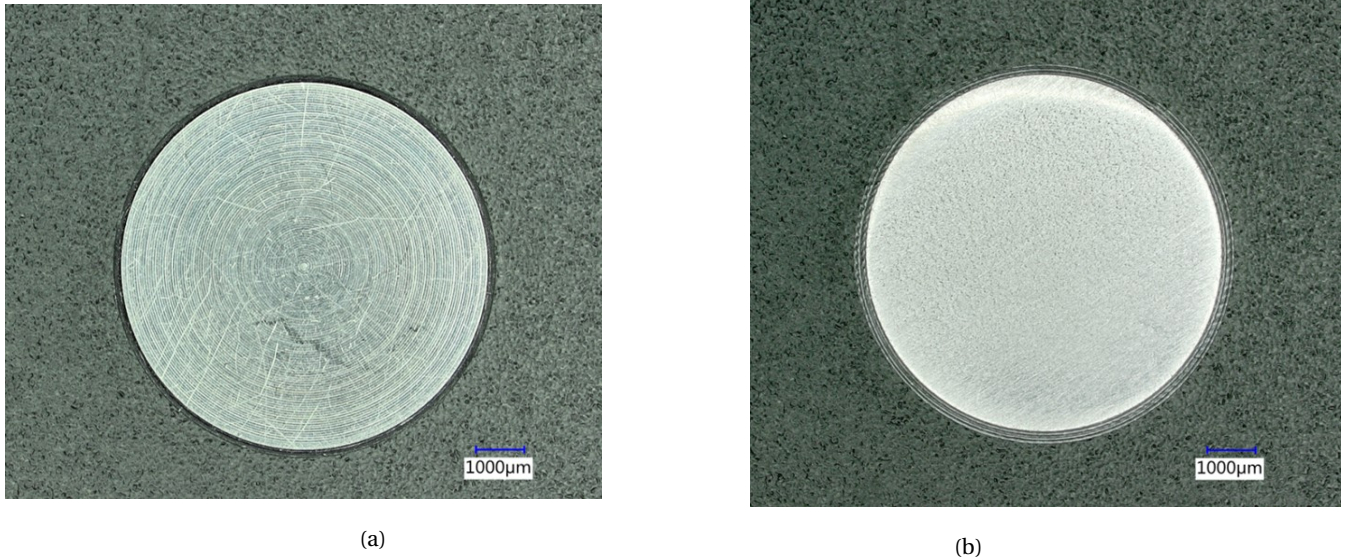


Figure 2.15: Discs manufactured for in vitro tests. Sub-figure (a) represents the machined surface and sub-figure (b) represents a P4000 grit polished surface.

mm feed per revolution was achieved under a cooling mixture of absolute ethanol (VWR International Lot: 19B064011) and air. In total, 203 discs were produced. The machined surface of the disc is shown in sub figure (a) of Figure 2.15. 30 of these samples were cleaned with acetone in an ultrasonic bath for 3 min twice and kept aside for degradation. The degradation method is given in section 2.3.2. Remaining 173 samples were polished using a grade 1200 and then a grade 4000 SiC abrasive paper from Struers. The grade P4000 grinding paper corresponds to a grain size of 5  $\mu\text{m}$ . This polished surface is shown in sub figure (b) of Figure 2.15. These 173 samples were washed with acetone in an ultrasonic bath for 3 min twice and dried. From the 30 degraded samples 3 were kept aside for observation and 3 from the 173 machined. A degraded sample is shown in section 2.3.2. Overall 197 samples were sent for gamma sterilization at 25 kGray to Mediscan GmbH & Co KG, Vienna.

#### 2.4.2. Cell bank preparation

For all tests, human dermal fibroblasts were used. The cells received from the Skin Engineering Platform at CABMM were frozen in liquid nitrogen in 2016 at the 4<sup>th</sup> passage. These were then thawed and counted. The counting was done on a NucleoCounter<sup>®</sup> and the cells showed a count of 3.1 million cells/ml at 98.6% viability. These were then seeded at 1900 cells/cm<sup>2</sup> in 20 T75 flasks for 8 days. On the 8<sup>th</sup> day, they were collected and counted. The total cell count recorded was 100 million cells which were then frozen at -80 °C. All further tests would receive their cells from this prepared bank. The cell culture media used for the cell bank preparation and all further experiments was prepared with high glucose DMEM (Gibco - R41965039), supplemented with 10% FBS (EU - Lot 41G3420K), 1% Penicillin/Streptomycin (Sigma - P4333) and 1% L- Glutamine. In further sections culture media refers to this composition.

### 2.4.3. Indirect contact assay

This test aims to assess the influence of the leachables on cell proliferation and viability. It allows both quantitative and qualitative analyses [39]. To achieve the same, gamma sterilized implant discs of 8 mm x 2 mm were placed in cell culture media, following the recommendation in ISO 10993-12 of surface area to extraction media ratio of 1.25 cm<sup>2</sup>/ml. The extraction was performed at 37 °C, in a humidified environment at 5% CO<sub>2</sub> for 72 h. These unfiltered extracts (medium containing leachables) were then added at various concentrations (diluted in fresh growth media) in 24 well culture plates, shown in Table 2.4 to cells cultured for 24 h at seeding density 4000/cm<sup>2</sup>. The experimental plan is illustrated in Figure 2.16. The plating plan is illustrated to indicate the placement of the different concentrations and replicates for each condition. The control used in this experiment was fresh culture medium, labelled as 0% concentration of extract. The cells were then observed after day 1, 2 and 3 by DNA quantification using Quant-iT™ PicoGreen® assay and after day 1 and day 3 by LIVE/DEAD® Viability/Cytotoxicity assay, both kits were from Molecular Probes®. The procedures for these are given below.

- **DNA quantification:** The adherent cells were lysed using 500 uL of 1% Triton X-100 solution. Triton X-100 is a detergent that permeabilizes the cell membrane and allows the cell contents to be released including DNA. This liquid was then collected and frozen in vials at 4 °C until all observation points were collected. These were then quantified using Quant-iT™ PicoGreen® which binds to double stranded DNA and produces fluorescence which was measured by a Tecan infinite® M200 plate reader. DNA quantification was used as an indication of cell number. Statistical analysis was performed using a one way ANOVA and Bonferroni Post- hoc test on IBM® SPSS® Statistics 23. A significant difference is defined for  $p < 0.05$ .
- **LIVE/DEAD® Viability/Cytotoxicity assay:** The stain was prepared as per the manufacturer's instructions, indicating a 2 mM Ethidium homodimer-1 (EthD-1) and 4 mM Calcein AM solution in phosphate buffered saline (PBS). EthD-1 binds to nucleic acids in cells with damaged membranes and emits a bright red fluorescence indicating dead cells. Non fluorescent Calcein AM turns fluorescent green when it is enzymatically converted by binding with live cells. The culture wells were washed with PBS and 1 ml of the above stain solution was added to the wells and observed under red and green fluorescent channels to observe the Calcein at 494/516 nm and the EthD-1 at 528/617 nm of the Leica DMI6000 microscope.

### pH measurement for indirect assay extract conditions

This test was performed to measure the pH of the extracts after exposing the implant discs to culture media after 24 and 72 h. This is aimed to provide information regarding the increase in pH at these time points and to measure the pH that was exposed to the cells at the start of the indirect contact assay. The same surface area/volume ratio of 1.25 cm<sup>2</sup>/ml was used for the extraction. The pH was recorded for culture media, and extracts of 100 %, 50 % and 10 % concentrations, diluted in

Concentration	Fresh Media	Extracts
0 %	100 %	-
10 %	90 %	10 %
50 %	50 %	50 %
100 %	-	100%

Table 2.4: Leachable preparation at different concentrations for the indirect contact *in vitro* experiment.

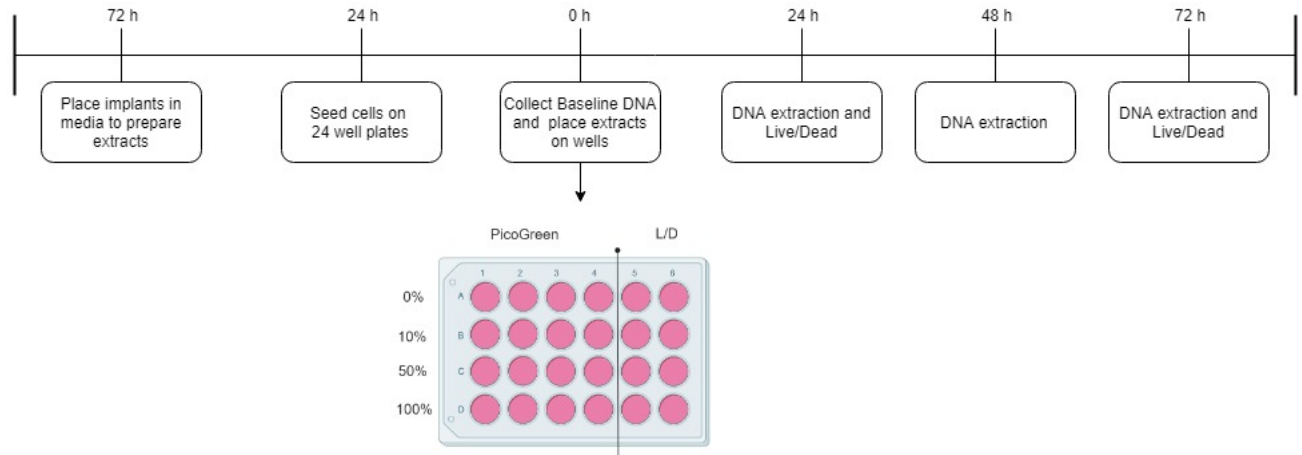


Figure 2.16: Indirect contact experiment plan with a representation of the culture plate. One plate was prepared per time point.

fresh media as in the indirect contact assay experiment. The pH was measured using a METTLER TOLEDO InLab<sup>®</sup>Expert Pro pH sensor.

#### 2.4.4. Direct contact assay

This test aims to observe the cell response when the implant is placed in contact with a confluent cell layer. As illustrated in Figure 2.17 cells were seeded at a high density of 8000 cells/cm<sup>2</sup>. After 24 h, a sterilized implant disc was placed on the layer of cells and stored at 37 °C, 5% CO<sub>2</sub> for 72 h. Three conditions of implants were tested in this experiment. i) polished implant discs after sterilization, from now on referred to as non degraded implants, ii) sterilized SBF degraded implant discs as seen in Figure 2.12 and iii) implant discs left over from the indirect contact experiment, here on referred to as DMEM degraded implant discs. At the end of the 72 h incubation period, the culture was stained as per the LIVE/DEAD<sup>®</sup> staining method elaborated in sub section 2.4.3.

#### 2.4.5. Direct seeding assay

This test aims to assess cell attachment to the implant surface. The culture wells were coated with Sigmacote<sup>®</sup> to ensure cells have only the implant surface as a possible attachment site. As illustrated in Figure 2.18 cells were seeded on the implant surface in a 50 µL suspension of 4000 cells/cm<sup>2</sup>. On the corner of the wells a drop of liquid was placed to prevent loss by evaporation. This set up was allowed to rest in the incubator for 20 min, to allow the cells to sediment at 37 °C, 5% CO<sub>2</sub>. After

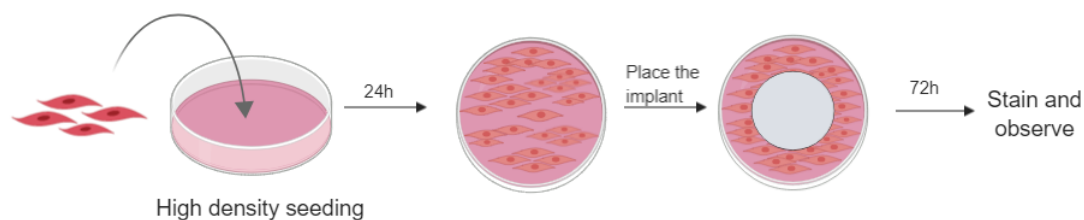


Figure 2.17: Direct contact experiment plan showing implant placement on a confluent cell layer.

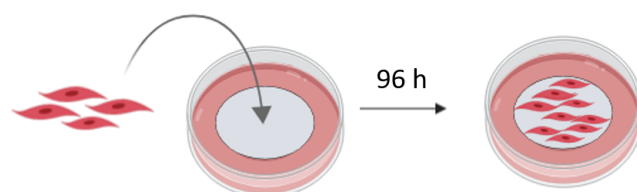


Figure 2.18: Direct seeding experiment plan showing cells cultured on top of the implant surface.

this period, 2 ml cell culture media was added from the sides to not disturb the implant and the wells were stored in the incubator for 4 days. Two implant conditions were tested this way, i) non degraded implants and ii) SBF degraded implants. At the end of the day 4 incubation period, the culture was stained as per the LIVE/DEAD<sup>®</sup> staining method elaborated in sub section 2.4.3.





# 3

## Results

### 3.1. Implant designing

#### 3.1.1. FE analysis

The 4 point bending simulation performed till the Ti model failed. The load was incremented in steps of 5 N and for a load case of 55 N, the Ti plate model showed high stress concentrations, indicating failure of the material. Therefore, for this load case, ZX10 plate dimensions were altered until for the same load, the ZX10 showed an acceptable stress condition (not failed). Figure 3.1 represents the Von Mises stress patterns obtained for the ZX10 plate and the Ti plate. The figure shows the top surface of the plate where the force was applied and the bottom which was constrained. The area near the constraints shows high stress concentration, as expected. The colour bars indicate the Von Mises stress present in the loaded plate with red indicating the highest and blue indicating the least stress. The scale of the color bar is set to indicate the highest stress for the tensile yield strength of the material. Figure 3.2 shows the displacement observed in the two plates for the same load case. The ZX10 plate showed a maximum displacement of 0.18 mm and the Ti plate showed a maximum displacement of 0.15 mm. The images represent a 0.5x exaggerated condition for easy visual interpretation.

#### 3.1.2. Final design of the implants

The final design of the screw is shown in Figure 3.3a. Its final length is 6.5 mm, outer diameter is 2.7 mm, inner diameter is 2.1 mm and the screw head is 4 mm in diameter. The final design of the plate is shown in Figure 3.3b. Its final length is 30 mm and the thickness is 1.55 mm. The CAD drawings for both parts are provided in Appendix B. Figure 3.4 shows the screws and plates in assembly and illustrates the 15° angular insertion allowance.

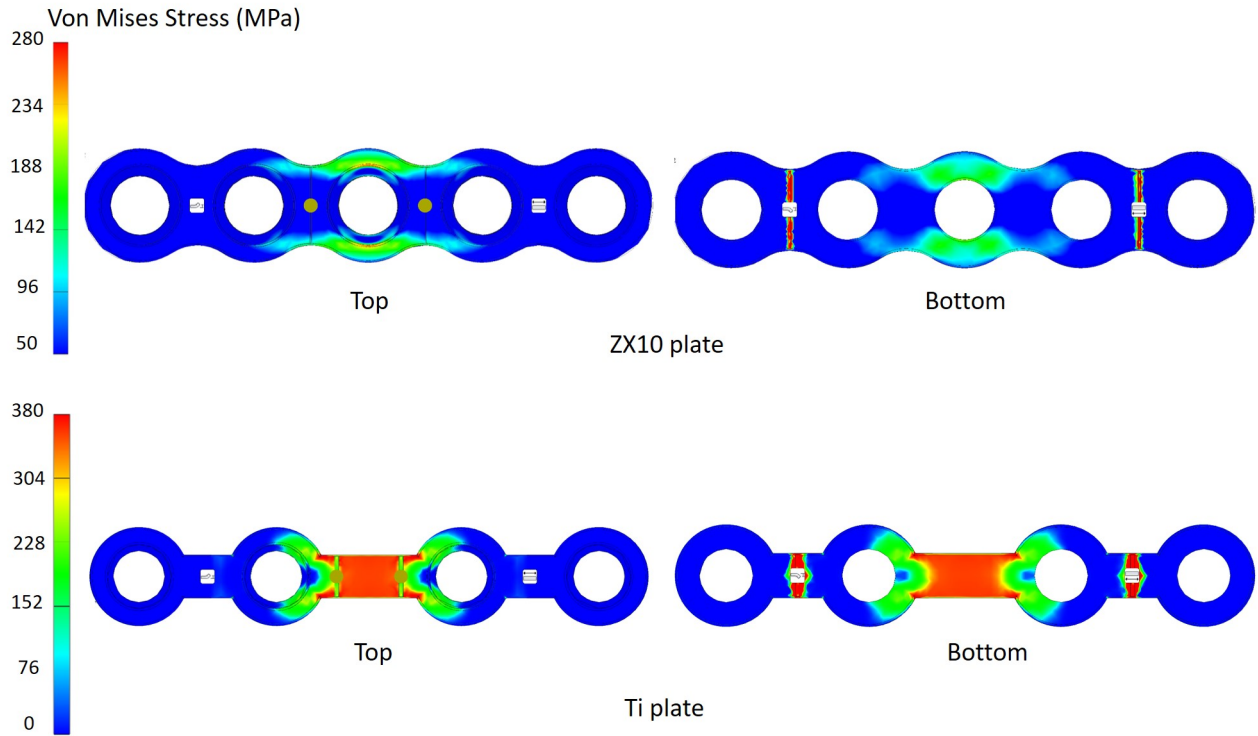


Figure 3.1: Von Mises stress patterns obtained for ZX10 plate and the Ti plate for a load case of 55 N. Top and bottom indicate the stress on the respective surface of the plate where the load and constraints were applied.

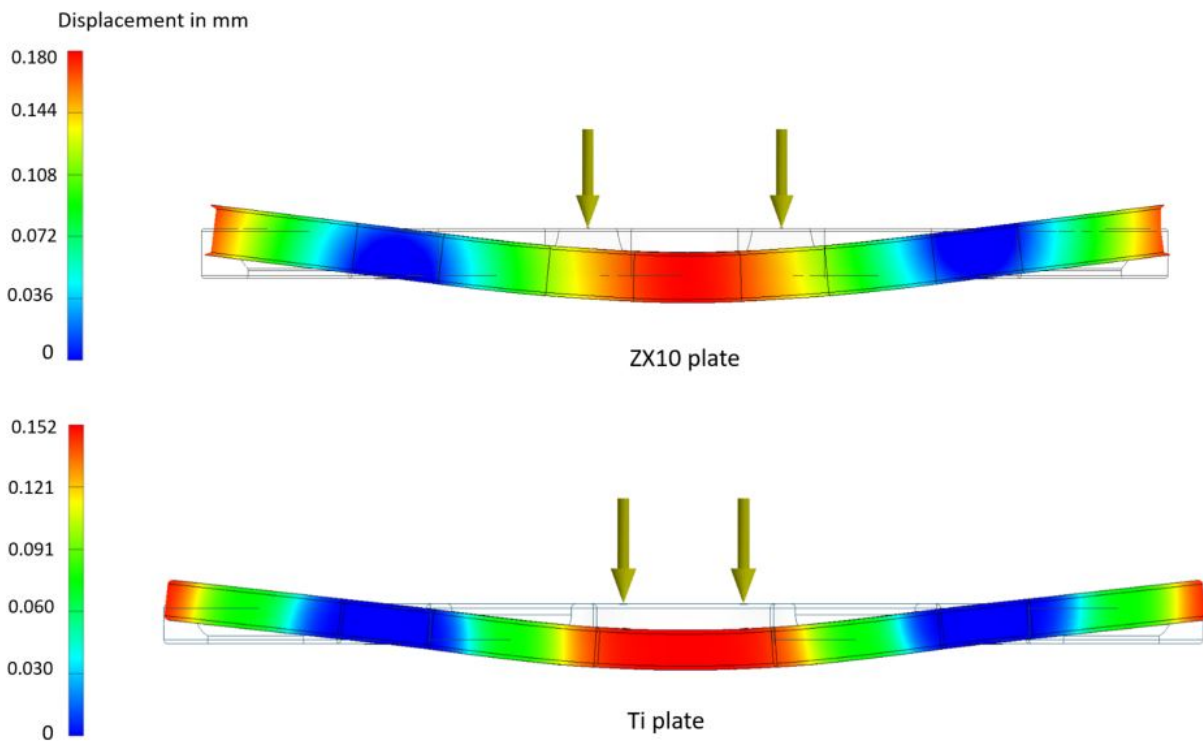


Figure 3.2: The displacement observed for a load case off 55 N for the ZX10 plate and the Ti plate. Images represent the actual representation x 0.5.

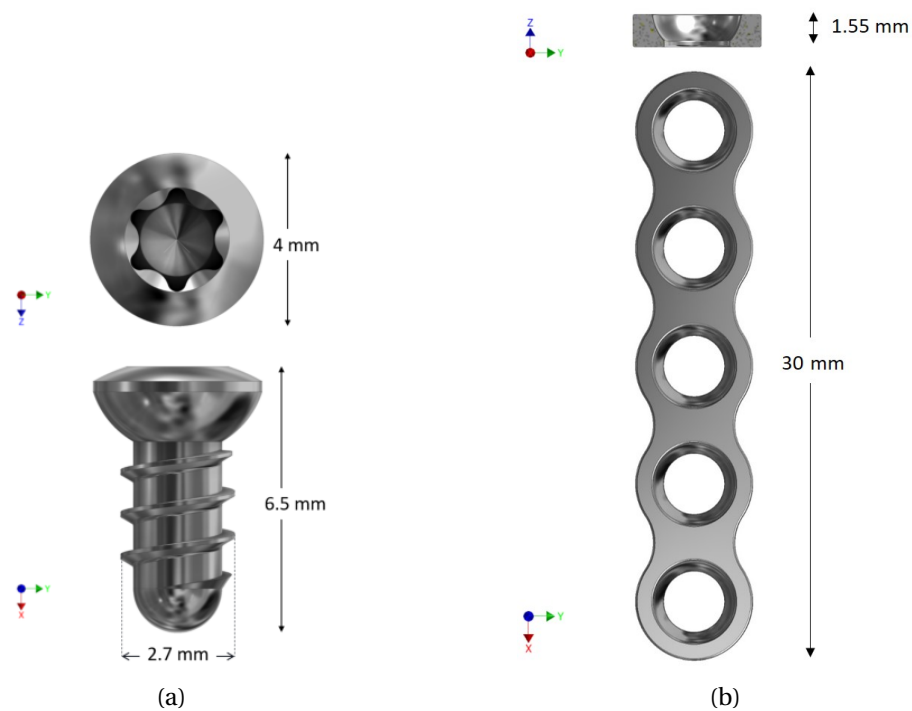


Figure 3.3: Final design of the screw (a) and plate (b). Figures not to scale.



Figure 3.4: Assembly of the screw plate system showing orthogonal screw and screw inserted at 15°.

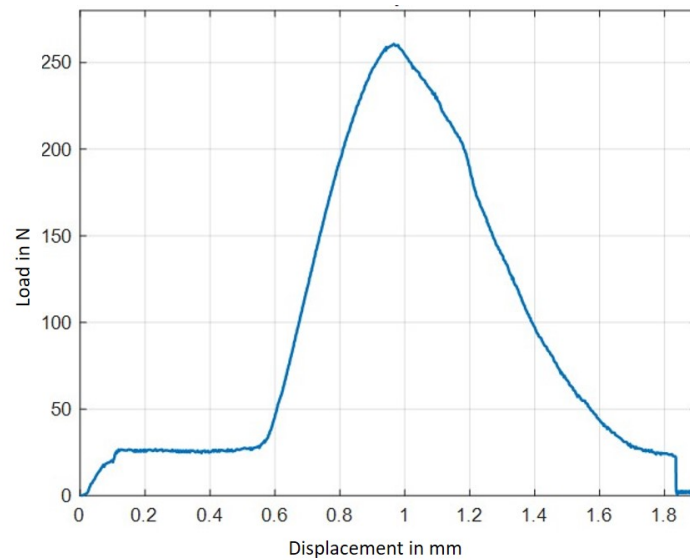


Figure 3.5: A typical pull out graph showing load in N vs displacement in mm for a ZX10 screw.

## 3.2. Mechanical testing

### 3.2.1. Pull out tests

The test was performed successfully as per the method in section 2.3.1. All samples of Mg and Ti showed expected pull out behaviour as shown in Figure 3.5. The initial increase in load noted for the first  $\approx 0.1$  mm of displacement is an artifact of the testing machine, where it loads to maintain the set up in tension and to avoid movement within its parts. Since the pull out force depends on the insertion depth, the pull out force was normalized to the insertion depth for each Mg sample, after adjusting for non threaded length (bottom of the screw accounting for 1.05 mm and 10 % to account for the crest of the flank). The Ti screw was completely threaded. For Mg, 7 samples were tested and for Ti, one sample was tested 6 times. From these normalized forces, the average and standard deviation was recorded and a comparison was drawn, as seen in Figure 3.6. The ZX10 screws recorded a mean pull-out force of 71.26 N/mm with a standard deviation of  $\pm 10.27$  and Ti screws recorded a mean pull-out force of 40.97 N/mm with a standard deviation of  $\pm 6.19$ . The failure in all cases was due to bone breaking and good bone-implant contact was seen established. A typical failed Mg screw is shown in Figure 3.7. Subfigure (a) shows how the bone failed in the threads and subfigure (b) in a higher magnification confirms that the screw threads were not sheared off. Some metallic colour was noted on the bone, which could be attributed to loose material from manufacturing because the sample was not cleaned after manufacturing and no defects were observed on the sample after pull-out. Kozakiewicz et al measured on average 55.01 N/mm for the commercial screws [37]. Since no information about the thread geometry was given, the pull out strength without accounting for the crest of the flank in the Mg screw was calculated as 64.13 N/mm with a standard deviation of  $\pm 9.6$ .

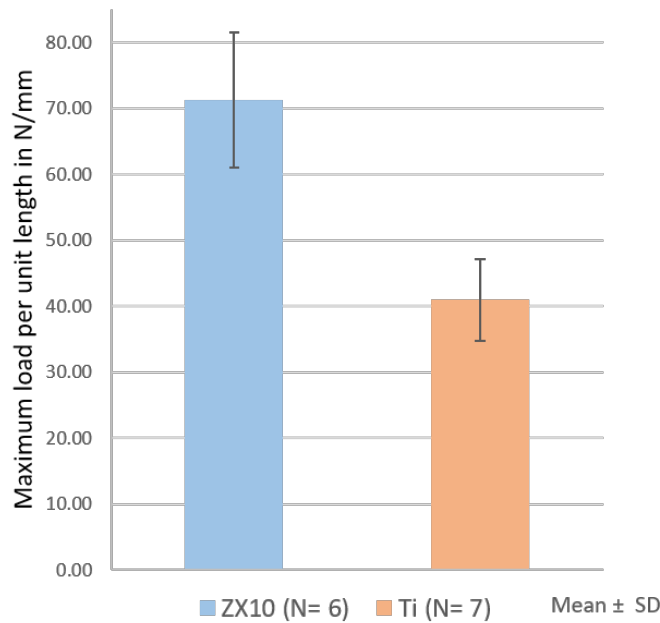


Figure 3.6: Pull out strength recorded for Ti and ZX10 screws, normalized to insertion depth of threaded length. The value represents the mean of N samples and error bars represent standard deviation.



(a)



(b)

Figure 3.7: ZX10 screw after pull out testing as observed by high resolution microscopy. The screw head was not manufactured as it was not required for the test. Subfigure (a) shows the whole screw and Subfigure (b) shows a magnified view which confirms there was no shearing of the screw threads.

### 3.2.2. 4-Point bending

The test was performed successfully as per the method in section 2.3.3. All samples of ZX10 showed similar ductile behavior as shown in Figure 3.8. A typical graph observed in all ZX10 4 point bending samples is shown in Figure 3.9. The yield values recorded from the experiments are reported in Table 3.1 and plotted in Figure 3.10. The abscissa of the graph represents weeks. Week 0 indicates non degraded samples. Values are plotted for 4 weeks for batch A12-C03-R2 and 8 weeks for batch A12-CO3-R3. No difference was expected between these two batches and this could be verified

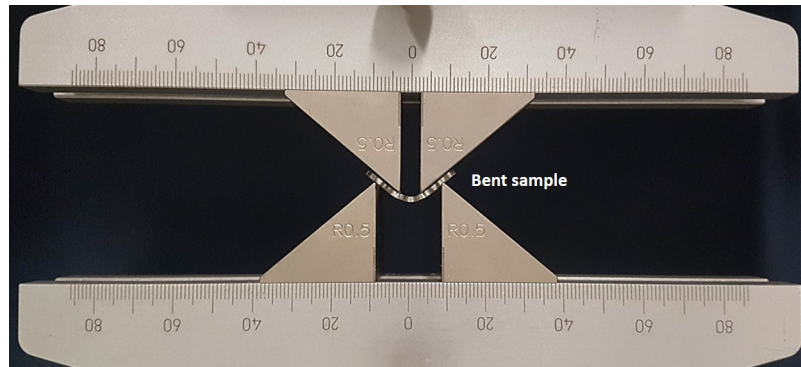


Figure 3.8: The figure shows a ZX10 sample that underwent loading and bent in a ductile manner. All tested samples showed similar behaviour.

in the 4 point bending yield load values, plotted on the ordinate. For both batches, 2 samples were tested for each time point. As expected, the yield load tends to decrease with increase in degradation time. After 4 weeks the rate of loss in strength seems to stabilize. The Ti plate showed a yield load of 28.6 N for the one sample that was tested and also showed ductile behaviour. Due to availability, only one sample could be tested.

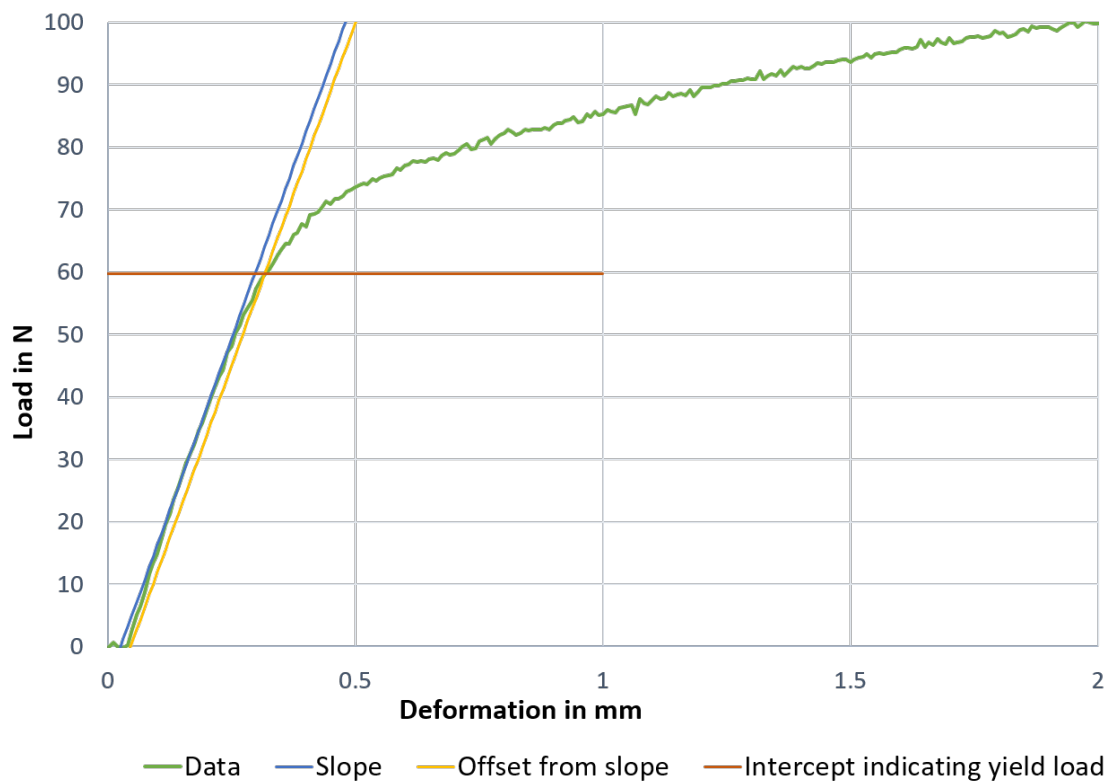


Figure 3.9: A typical 4 point bending graph showing load in N vs displacement in mm for a ZX10 plate (Green). The yield load (red) was estimated by calculating the slope (blue), drawing a line having an offset of 0.02 mm (yellow) from the slope and checking the intercept.

	A12-C03-R2		A12-C03-R3	
	Yield load (N)	Stiffness (N/mm)	Yield load (N)	Stiffness (N/mm)
Non degraded samples	64.69	308.64	59.8	253.33
	59.82	200	58.58	225
SBF- 1 week	59.18	201.24	49.11	257.14
	56.49	201.24	50.62	225
SBF- 2 weeks	42.29	178.02	43.97	197.56
	45.37	198.77	44.78	197.56
SBF- 3 weeks	38.89	179.99	39.93	180
	37.66	185.15	33.49	149.31
SBF- 4 weeks	37.71	128.57	34.62	129.08
	35.4	128.57	36.89	149.31
SBF- 5 weeks			24.12	105.88
			24.18	85.71
SBF- 6 weeks			26.41	100.87
			22.98	120
SBF- 7 weeks			25.01	92.90
			25.62	98.18
SBF- 8 weeks			20.83	73.22
			10.7	35.76

Table 3.1: Table represents force values and corresponding stiffness recorded for non degraded and degraded plate samples of two batches (A12-C03-R2 and A12-C03-R3) in 4 point bending. Value represents the loads at which the material plastically deforms (Yield point) and corresponding stiffness. Two samples were recorded for each condition of each batch.

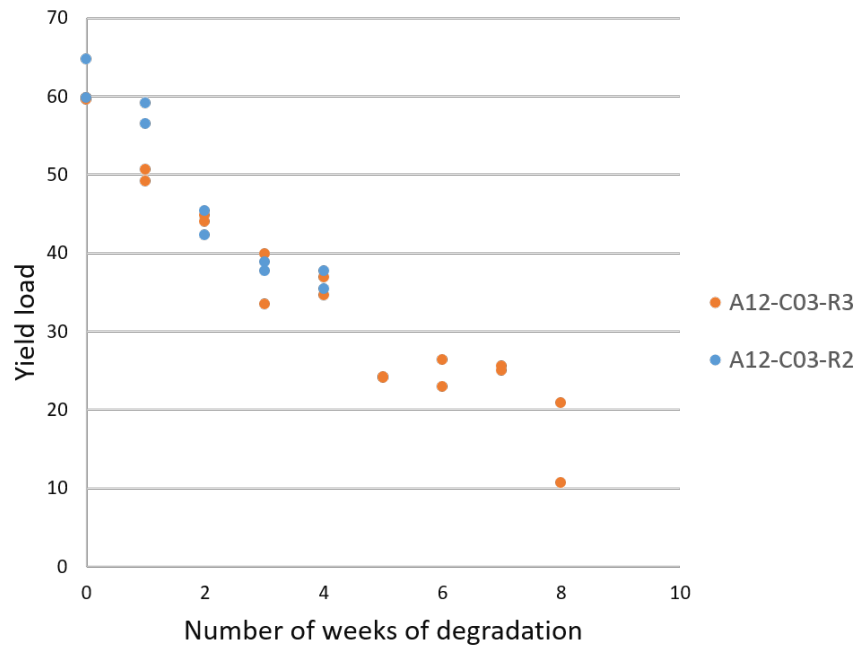


Figure 3.10: Graph represents the yield load in 4 point bending tests for 2 samples of each batch. Non degraded samples and samples degraded in SBF were tested after every week, upto 4 weeks for batch A12-C03-R2 and upto 8 weeks for batch A12-C03-R3.

### 3.2.3. Degradation by immersion in SBF

The weight of the samples recorded after removal of corrosion products is reported in Table 3.2. From this the degradation rate by mass loss is calculated using equation,

$$CorrosionRate = \frac{W}{A.t.\rho} \quad (3.1)$$

where,  $W$  is the mass loss recorded,  $A = 340.99 \text{ mm}^2$  is the surface area exposed to the fluid,  $t$  is time and  $\rho$  is density, taken as  $1.738 \text{ g/cm}^3$ . The degradation rates over 8 weeks of degradation in SBF is presented in Figure 3.11. From the average of the samples at 8 weeks of degradation, a degradation rate of  $1.08 \text{ mm/year}$  could be calculated. From the data presented in Figure 3.11 and from the 4 point bending yield load values presented in Figure 3.10 it could be confirmed that there is no difference between the two batches of material, as expected.



	Weight in g	
	A12-C03-R2	A12-C03-R3
Non degraded samples	0.2530	0.2556
	0.2535	0.2554
SBF- 1 week	0.2423	0.2426
	0.2425	0.2427
SBF- 2 weeks	0.2362	0.2340
	0.2335	0.2351
SBF- 3 weeks	0.2229	0.2180
	0.2226	0.2235
SBF- 4 weeks	0.1989	0.2072
	0.1950	0.2068
SBF- 5 weeks		0.1885
		0.1777
SBF- 6 weeks		0.1873
		0.1885
SBF- 7 weeks		0.1811
		0.1813
SBF- 8 weeks		0.1694
		0.1444

Table 3.2: Mass losses recorded for two samples of two batches of ZX10 plate samples, over 4 weeks for batch A12-C03-R2 and 8 weeks for batch A12-C03-R3. The samples were degraded in SBF, the corrosion products were removed and then weighed.

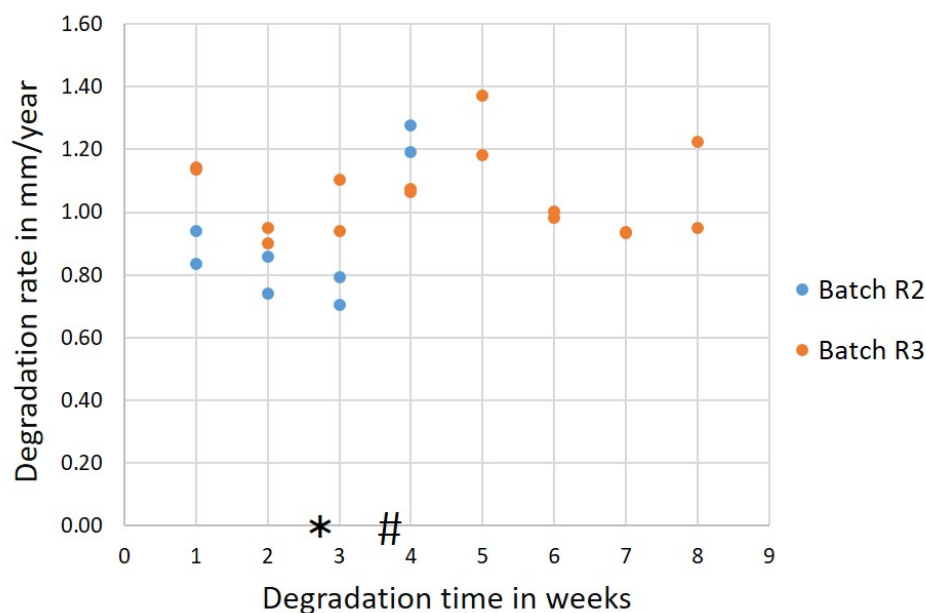


Figure 3.11: Degradation rates recorded for each sample after every week of degradation upto 8 weeks in SBF. The corrosion rate for each sample is calculated for the whole period of degradation up until that point. R2 represents batch A12-C03-R2 and R3 represents batch A12-C03-R3. The symbols '\*' and '#' denote the discrepancies in temperature and pH noted in the set up, respectively, due to equipment malfunction as elaborated in previous sections.

### 3.3. *In vitro* tests

#### 3.3.1. Indirect contact assay

The assay was run successfully as elaborated on in the methods section with differences noted in results and established against the controls. Quantitative results were recorded for the assay by DNA extraction and subsequent use of PicoGreen<sup>®</sup> stain, and qualitative results by phase contrast microscopy and LIVE/DEAD<sup>®</sup> viability and cytotoxicity assay. These are further elaborated on below.

- Quant-iT<sup>™</sup> PicoGreen<sup>®</sup>: For the Pico green assay, as per protocol, a standard curve was calculated. The DNA concentrations corresponding to emission were extrapolated and used to quantify the amounts of DNA in the samples. Figure 3.12 illustrates the cell viability for the different extract concentrations with 0 % as the baseline condition. From the statistical test, the following result was recorded. On Day 1 (D1), a significant difference was noted between 0 % and 100 % extract group with  $p = 0.001$  and between 10 % group and 100 % extract group with  $p = 0.007$ . On Day 2 (D2), a significant difference was noted between 0 % group and 50% group with a  $p = 0.001$  and between 0 % and 100 % group with  $p = 0.000$ . No significant difference was observed between 0% and 10 % groups but a difference was noted between 10 % group and 50 % group with  $p = 0.012$  and between 10 % group and 100 % group with  $p = 0.001$ . On Day 3 (D3), a significant difference was noted between all groups. Between 0 % and

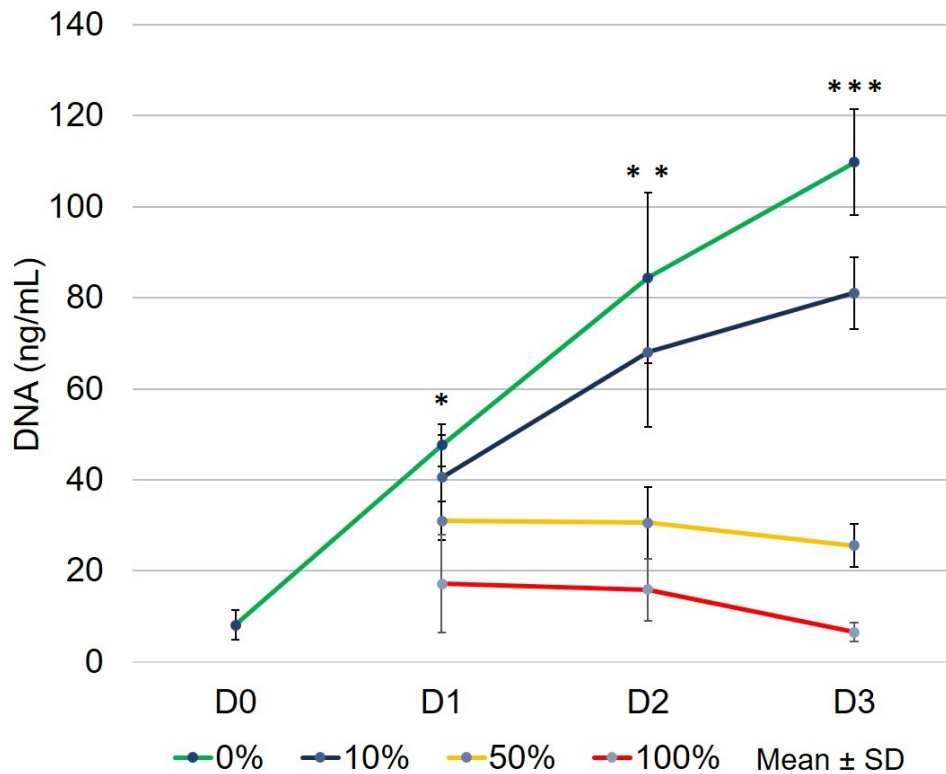


Figure 3.12: Cell proliferation and viability recorded by DNA quantification using Quant-iT™ PicoGreen® for different concentrations of extracts in the indirect contact assay. Results represent the mean of experimental quadruplets and technical triplicates. Error bars represent one standard deviation. Symbol '\*' on D1 time-point represents a significant difference between 0 % and 100 % extract group with  $p = 0.001$  and between 10 % extract group and 100 % extract group with  $p = 0.007$ . Symbol '\*\*' on D2 time-point represents a significant difference between 0 % and 50% group with a  $p = 0.001$  and between 0 % and 100 % group with  $p = 0.000$ . Symbol '\*\*\*' on D3 time-point represents a difference between all groups. Between 0 % and 10 %, 50 %, 100% groups a  $p = 0.001$ ,  $p = 0.000$  and  $p = 0.000$  was noted, respectively. The 10 % groups showed a significant difference to 50 % and 100% group with  $p = 0.000$ . The 50 % group showed a significant difference to 100 % group with  $p = 0.023$ .

10 %, 50 %, 100% groups a  $p = 0.001$ ,  $p = 0.000$  and  $p = 0.000$  was noted, respectively. The 10 % groups showed a significant difference to 50 % and 100% group with  $p = 0.000$ . The 50 % group showed a significant difference to 100 % group with  $p = 0.023$ .

- **LIVE/DEAD®:** Phase contrast and Live/Dead cell images were recorded after 24 (Day 1) and 72 h (Day 3). The detailed images are reported in Appendix C. Figure 3.13 shows representative versions of the same. Day 1 observations showed cells viable and proliferating in all except the 100 % extract media. At that time point, between the 0 %, 10 % and 50 % groups visible difference's were not noted. On day 3 however, the 50% extract group showed visibly lower concentration of cells as compared to 0% and 10 % groups. The 100 % extract group showed similar trends to day 1 with very few viable cells. Due to a technical difficulty, only live channel results could be recorded. For qualitative morphological grading, ISO 10993-5 describes a mild cytotoxicity when not more than 50 % of the cell layers are lysed and a moderate cytotoxicity when not more than 70 % of the cell layers are lysed, but when more than 50 % of growth

is inhibited. A severe cytotoxicity is described, when there is a near complete destruction of the cell layers. From Figure 3.13 the 100 % extract condition showed severe cytotoxicity from Day 1 to Day 3.

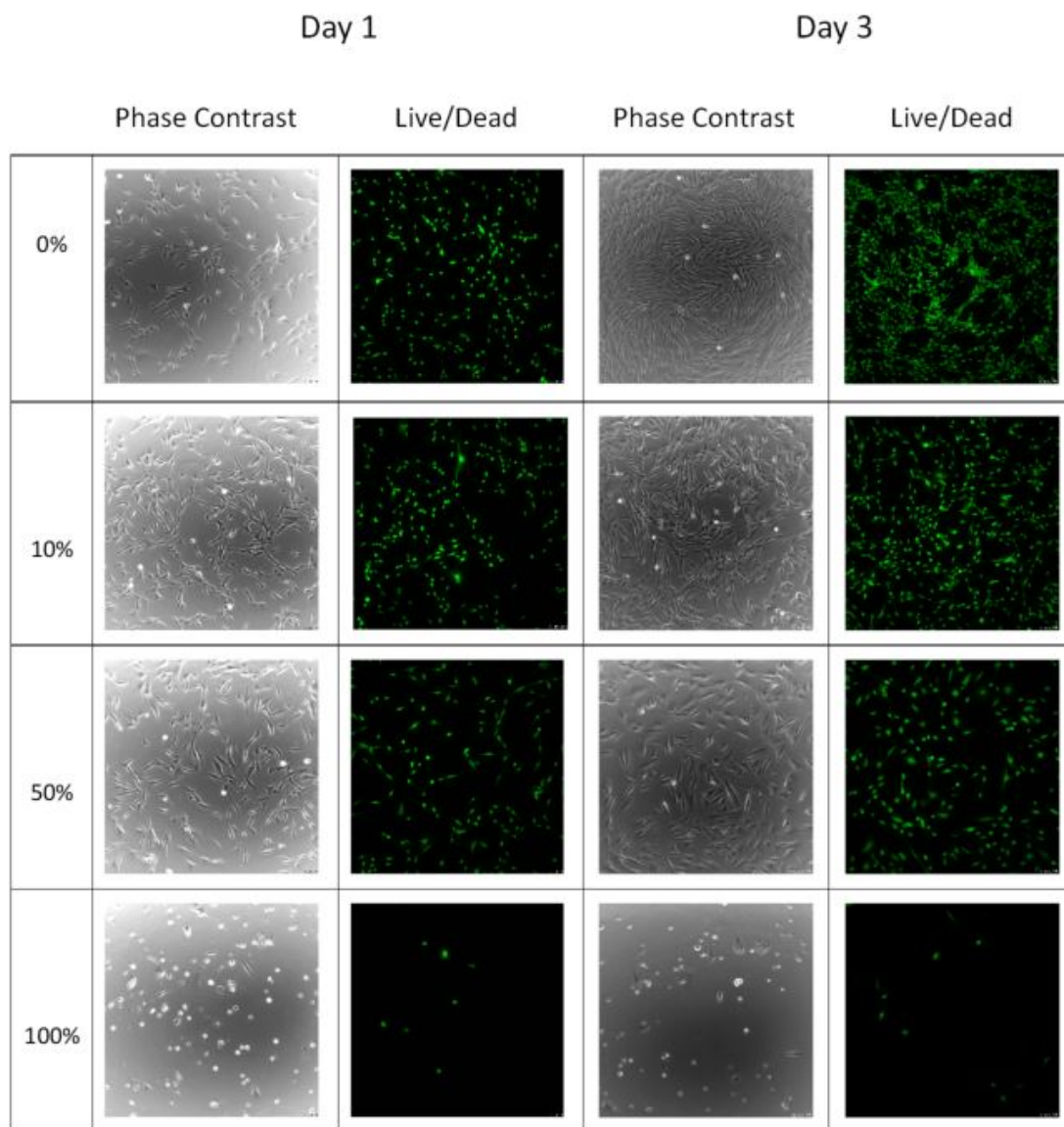


Figure 3.13: Phase contrast and LIVE/DEAD® assay after day 1 and day 3 of the indirect contact assay. Only the live channels are recorded due to a technical difficulty. Long spindle shaped cells of the phase contrast images indicate healthy cells and green spots from the Live/Dead study indicate live cells.

### pH measurement for indirect assay extract conditions

Table 3.3 shows the results recorded after day 1 and day 3 of implant exposure to the culture media. The result at the end of day 3 is believed to be the pH exposed to the cells at the start of the indirect contact assay.

Condition	Day 1 pH	Day 3 pH
0 % extract	7.75	7.78
10 % extract	7.84	8.11
50 % extract	7.95	8.32
100 % extract	8.04	8.31

Table 3.3: pH recorded after 24 h (Day 1) and 72 h (Day 3) of exposing implant discs to culture media in various concentration. The dilution was performed in fresh media.

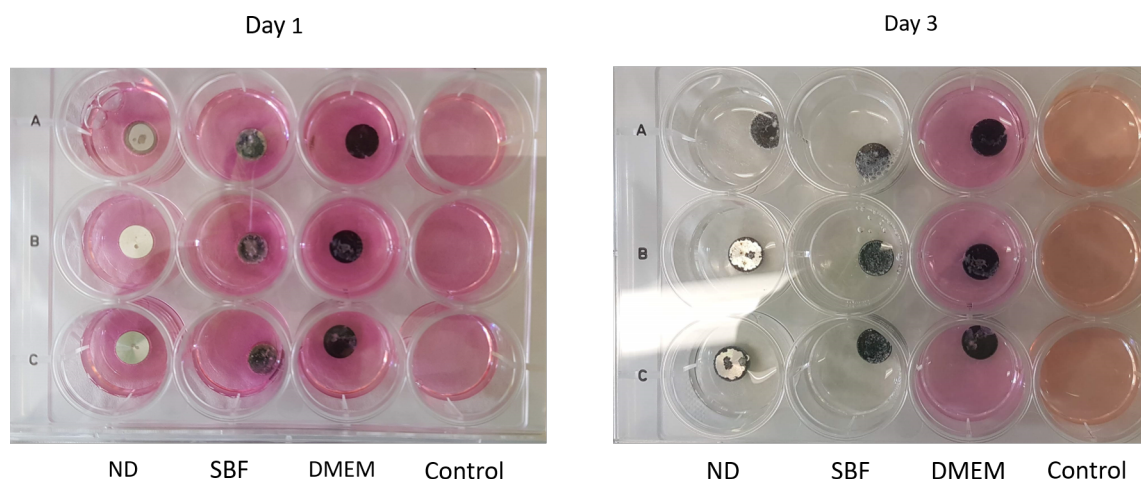


Figure 3.14: Direct contact assay culture wells showing change in colour after 3 days (right). ND represents non degraded implants. Control wells contain only cells.

### 3.3.2. Direct contact assay

The assay was run successfully as per methods elaborated on in earlier sections, however it was noted that the implant discs moved in the culture wells during the procedures and this may have introduced a variance in the results. Three samples of non-degraded, SBF degraded and DMEM degraded implant discs were tested by direct contact on a confluent cell layer. The controls used in this experiment were cultured cells with no implants. An interesting observation regarding the change in the colour of the culture media was noted at the end of this experiment with the media in non degraded and SBF degraded implant wells losing color as captured in Figure 3.14. Another interesting observation was noted with small crystal like degradation products seen on the culture well as shown in Figure 3.15. Wherever these were present in the wells, cells were not seen in that vicinity. They were observed in small concentrations in the media degraded implants and in abundance in the SBF degraded implant wells. The results from each of these experimental conditions are elaborated on below.

#### Control wells

These wells contained no samples and only cultured cells. All wells were characterized by many well attached spindle shaped live cells and few dead cells. Figure 3.16 represents the control well in bright field (sub-figure a) and fluorescent (sub-figure b) mode.



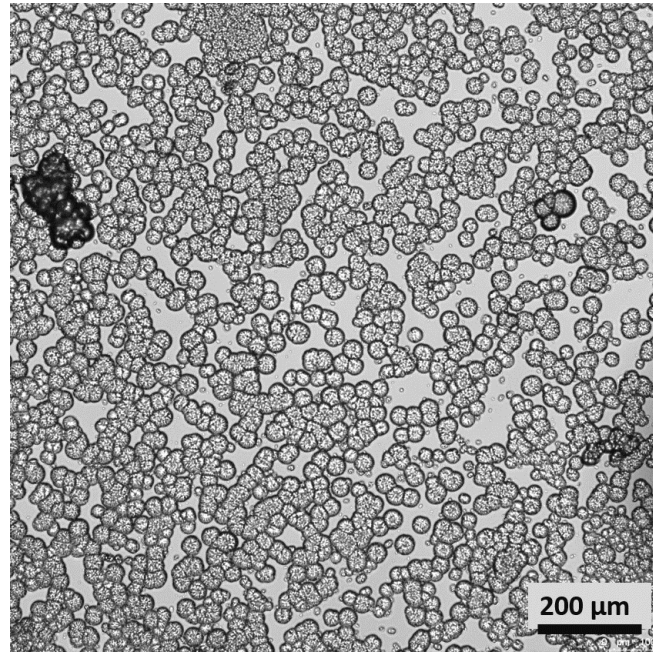


Figure 3.15: Observation of degradation products in the wells of the direct contact experiment.

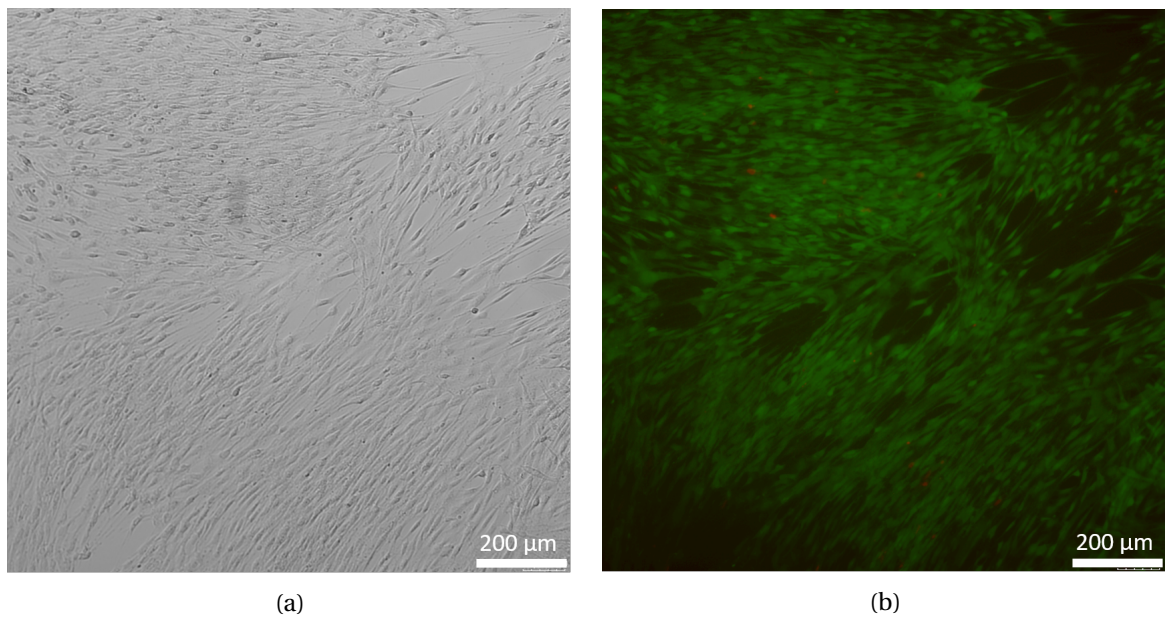


Figure 3.16: Control wells with no implant discs showing well attached and healthy looking cells in bright-field (a) and fluorescent (b) mode.

### Non degraded samples

Figure 3.17 represents a culture well imaged with the edge of the implant shown in the top left corner, appearing dark. In close vicinity of the implant, a few attached cells of spindle shaped morphology were noted and many round dying cells were seen. Sub figure (a) represents the well in bright field mode and sub-figure (b) shows the LIVE/DEAD<sup>®</sup> stain on the same position. Figure 3.18 represents the edge of the well, where cells show good confluence, more of spindle shaped mor-

phology and appear to have more normal growth, as seen in bright-field mode in sub figure (a) and fluorescent mode in sub figure (b).

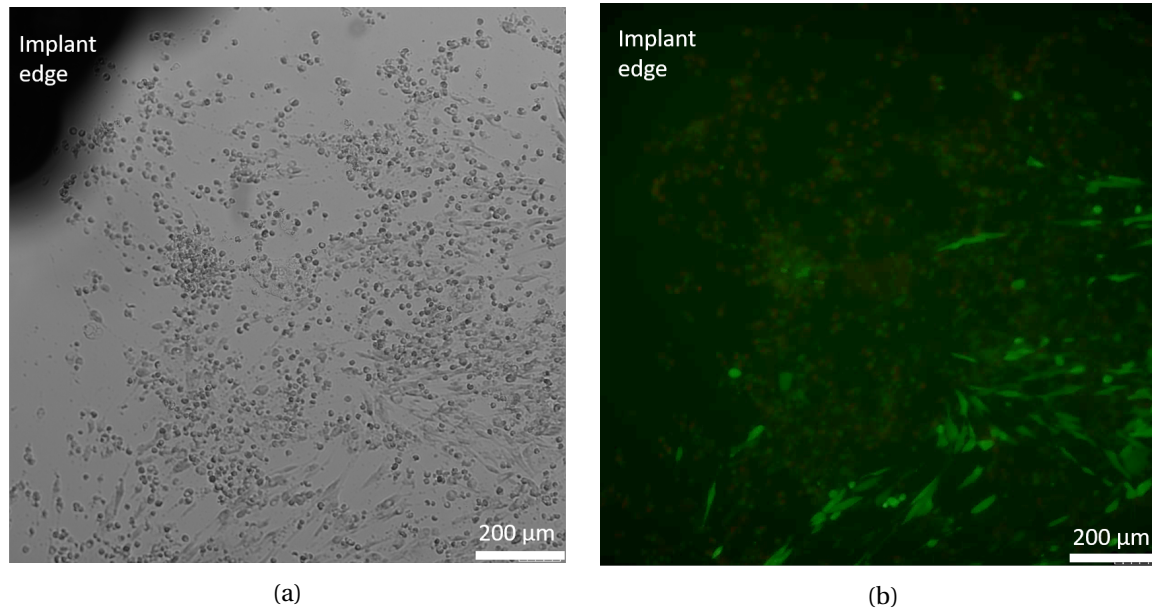


Figure 3.17: Non-degraded implants observed after 72 h on direct contact with cell layer. Sub-figure (a) shows rounded cells and few attached healthy looking cells and sub-figure (b) confirms the same with LIVE/DEAD<sup>®</sup> stain. Very mild green signal is seen in small spots indicating dying cells.

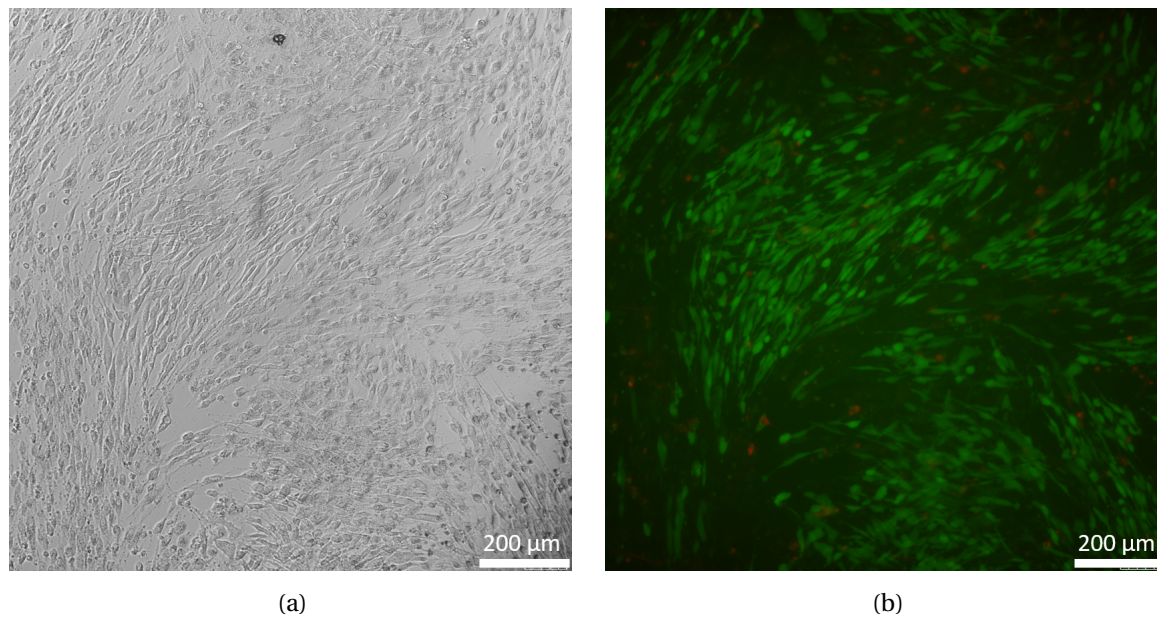


Figure 3.18: The edge of the culture well shows well attached healthy looking cells seen in bright field mode in sub-figure (a) and sub-figure (b) shows the same spot using fluorescent mode to visualize the LIVE/DEAD<sup>®</sup> stain. Live cells are indicated by green and dead cells by red spots.

### SBF degraded samples

In all three samples no healthy living cells were observed. Some dying cells and many dead cells were observed near the implant edge as shown in Figure 3.19. No living cells were spotted on the



edge of the wells either.

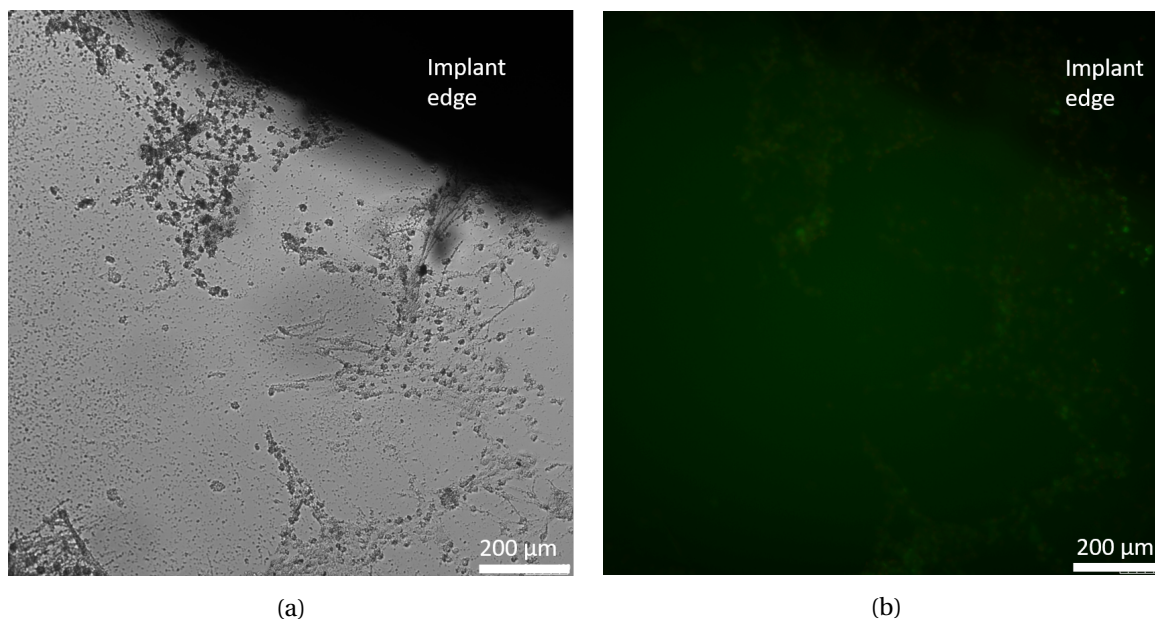


Figure 3.19: SBF degraded implants observed after 72 h on direct contact with cell layer. Sub- figure (a) shows cell debris and no visibly healthy cells and sub figure (b) confirms the same with LIVE/DEAD<sup>®</sup> stain. Very mild green signal is seen in small spots indicating dying cells.

### DMEM degraded samples

As shown in sub figure (a) and sub figure (b) of Figure 3.20, on the edge of the DMEM degraded implants, few living cells were spotted and many dying and dead cells were noted on all three samples. No cells were observed on the edge of the well. Interestingly all samples showed well attached and living cells under the implant surface. These results are shown in Figure 3.21.

#### 3.3.3. Direct seeding assay

This assay was performed as per recommended standards elaborated on in the methods section. However, for both non degraded and SBF degraded cases of testing, no cell attachment was observed. Figure 3.22 is a representative image observed in all cases showing bubbles on the implant surface (indicated by white arrows) and red signal indicating cell death. Out of three, one well of the non degraded implant turned transparent and both SBF degraded wells turned transparent. One of the SBF degraded wells showed many bubbles and appeared cloudy to the naked eye.



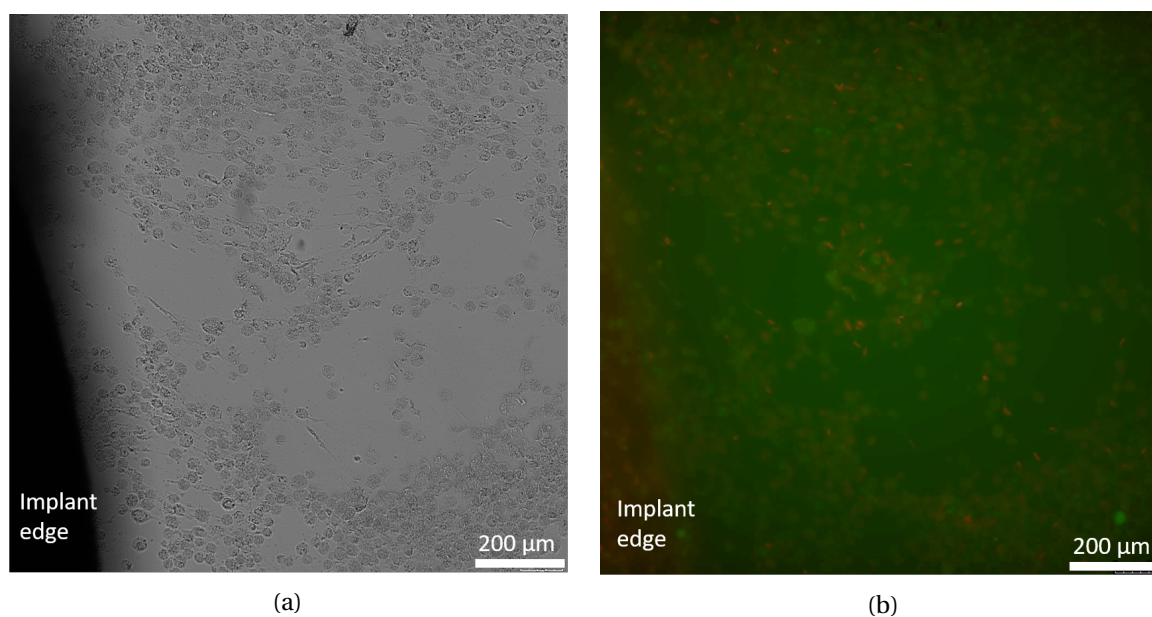


Figure 3.20: DMEM degraded implants observed after 72 h on direct contact with cell layer. Sub-figure (a) shows rounded and dying cells near the implant edge and sub-figure (b) confirms the same with LIVE/DEAD<sup>®</sup> stain showing many red spots.

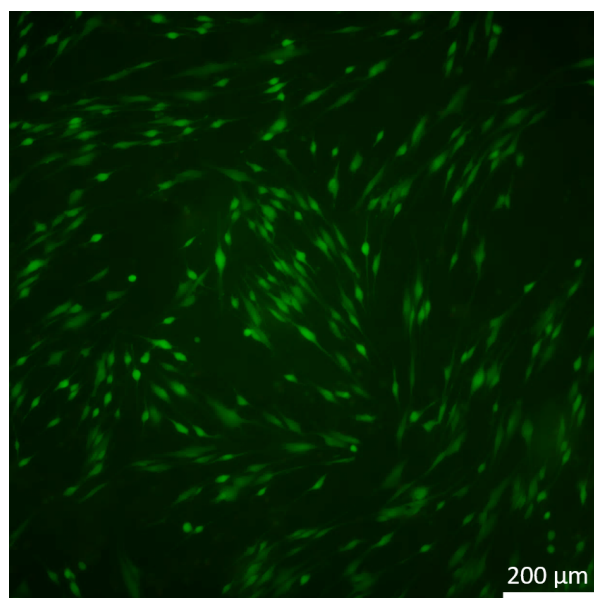


Figure 3.21: Well attached and healthy looking cells observed under the DMEM degraded implant surface.

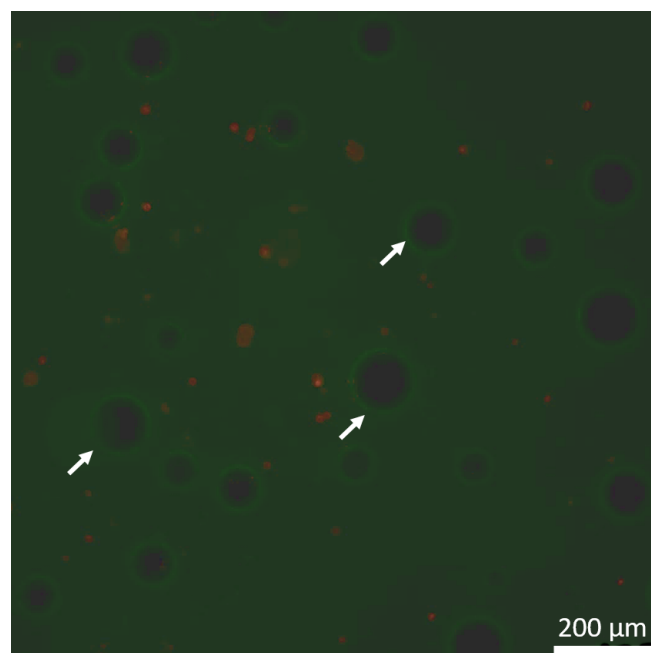


Figure 3.22: Non degraded implant surface after day 4 of direct seeding assay showing many bubbles indicated by white arrows and red signal of the LIVE/DEAD<sup>®</sup> stain indicating dead cells.

## Discussion

### 4.1. Mechanical tests

#### 4.1.1. Pull out test

Screw pull out from bone or bone like material often follows three kinds of failure modes, i) failure due to screw head breaking off, ii) failure due to the screw thread shearing off and iii) failure due to bone breaking [40]. Another possible failure mode is the combination of ii) and iii). In the current screw model the failure mode observed is due to the bone breaking. This type of failure is characterized by equation,

$$F = \pi d_0 t_t \tau_{\max} \quad (4.1)$$

where  $F$  is the pull out force by shear failure,  $d_0$  is the major diameter of the screw,  $t_t$  is the threaded length of the screw and  $\tau_{\max}$  is the shear strength of the bone. The shear strength of the artificial bone material used in this report is given as 11 MPa [41]. Therefore, for a screw of major diameter 2.7 mm and a 1 mm insertion leading to threaded length of 0.9 mm, after accounting for the crest of the flank, a pull out force of 83.93 N should be achievable. The mean pull out force for the ZX10 screws is 71.26 N with a SD of 10.27. Similarly for the Ti screws the maximum achievable force as per equation 1 is 47.728 N and in the experiments, a mean of 40.97 N with a SD of 6.19 was achieved. Apart from this, the analytical solutions assume an ideal case of perfect shear whereas in the experimental case, compressive forces on the flank, and the bone geometry also have influences on pull out force. It was also noticed that the pull out force variation might be related to the insertion speed and careful and extremely slow insertion led to apparent higher forces. This could be due to good engagement of the bone in the screw threads and due to less "wobbling". Since the screw head was not manufactured it is not possible to comment on torque transmission and its effects, but this is a parameter that should remain a point of consideration for future work. The process of inserting the screws should also follow the standardized methods. Increasing the pitch and outer diameter of

the screw could lead to maximized pull out forces as given by the relation in equation 4.1. However, the goal is not to maximize pull out forces alone, but to achieve maximum desired pull out force using minimum material and causing minimal damage to bone. The results for the ZX10 screws are quite optimal compared to the analytical solution based on achievable pull out strength for the given outer diameter, but the screws appear much stronger than the DePuy Synthes Ti screw in this study. The pull out force without accounting for the crest of the flank was 64.13 N/mm with a SD of 9.6 which is comparable to the Medartis screw (2 mm system, self tapping and 6 mm in length) measured in Kozakiewicz et al with a value of 63.55 N/mm. However, since the exact insertion depth of the screws was not given and only mentioned insertion length was, upto 3.6 mm, this comparison is not conclusive. Since the Ti screw used in this study is also an implant of the CMF region the results indicate a satisfactory first prototype, however, as it always possible to make the implant bigger and therefore stronger, care must be taken to avoid over dimensioning. A smaller dimension of outer diameter can be considered for the next prototype. Since Mg is a degrading material, this allowance of higher pull out force may account for the loss of strength over time. Apart from the experimental observations, the final design and dimensions of a real prototype must consider the quality of the bone specific to the patient as bone quality at site is an important factor that affects primary stability of the implant along with contact between bone and implant.

#### 4.1.2. 4 point bending test

All samples of ZX10 material showed good ductility which is desirable in fracture fixation. Over 8 weeks of degradation in SBF the yield load decreased from  $\approx 60$  N to 15 N. Since the yield load of the commercial Ti plate was measured as 28.6 N, at week 8, the ZX10 plate from *in vitro* degradation measures weaker. However, at this time point the fracture is expected to have healed and also, *in vitro* measurements are established to be faster than *in vivo* degradation [1] and therefore the results seem promising but not conclusive. A common fracture is expected to heal within 8 weeks [42] and it is important for the material to retain strength during the entire duration of healing. In the future it would be useful to measure the loss of strength in comparison to a WE43 system to accurately predict if the material behaves sufficiently. However, it can be established that the material can be acceptably dimensioned to achieve mechanical strengths required for CMF fixation.

The results for the ZX10 plate conformed well to the corresponding FE model. The Ti plate failed at approximately 28.6 N experimentally while in the FE model the predicted force value was 55 N. A possible reason for this could be that the material was modelled as a Grade 3 Ti which might have been an overestimation and in reality the plate could be Grade 2 which is commonly used in low load bearing regions. Considering this, the FE model was simulated again as a Grade 2 Ti with yield strength of 276 MPa and the model failed at 40 N. The flexural strength was also calculated analytically and the value recorded was 257.4 MPa which also relates closely to the yield strength of Grade 2 Ti. Microstructural analysis is required to accurately assess the material composition and strength for future adaptations. The measured stiffness for the Ti plate is 138.6 N/mm and in

the FE model is 392.8 N/mm. For the ZX10 plate the experimental stiffness noted is 246.74 N/mm by taking the mean of the 4 non degraded sample and in the FE model is 392.85 N/mm. The high stiffness values recorded in both FE models can be attributed to the shear locking phenomenon observed in linear tetrahedral elements which is characterized by a sharp increase in elemental stiffness. It is commonly advised to avoid using these elements in bending problems, however the the software used in this study does not allow other meshing possibilities [43]. Higher order reduced integration elements available on other softwares should be able to account for this discrepancy. Another reason for the high stiffness in the FE model can be the "fixed" constraint used, however this would not explain the very large difference observed and the meshing element is the more probable cause.

#### 4.1.3. Degradation in SBF

Degradation tests popularly performed to assess degradation rates depend specifically on the conditions of the experiment conducted and the test material conditions. Properties such as exact composition of the degradation liquid, pH of the electrolyte, composition of the Mg alloy, surface condition of the material all have significant impacts on the degradation rate [44]. Therefore, the most accurate comparison that can be drawn is to the material tested in the same group with the same SBF and experimental conditions. The value reported in this report is not conclusive for the material as discrepancies in temperature and pH were noted due to malfunctioning of the equipment as mentioned in earlier sections. In previous experiments with ultrahigh-purity ZX10 a corrosion rate of approximately 2 mm/year was recorded which is not too far from the 1.08 mm/year seen in this report. Imwinkelried et al [45] analyzed a WE43 system which is now CE approved and measured a degradation rate of 1.6 mm/year in their static SBF immersion and the same material *in vivo* showed a degradation rate of 0.4 mm/year. *In vitro* degradation rates have been speculated to be much higher than *in vivo* degradation rates in various Mg alloys [44, 45] but the test is still a useful tool to measure material improvement and draw comparisons to commercially established degradable materials.

## 4.2. Implant designing

From the mechanical tests performed, certain conclusions can be discussed regarding the design of the implant parts. Both screw and plate followed initial recommendations of a surgeon and followed simple implant designs as observed regularly in commercial systems. Since Mg has a much lower yield strength as compared to Ti, it was necessary to dimension the screw with a larger outer diameter and the plate thicker. In the case of the screws, from the pull out results it became clear that the screw could achieve a much higher pull out force as compared to a Ti screw. If the material can retain sufficient mechanical strength over the course of fracture healing then a screw of smaller outer diameter could be envisioned. Unfortunately from the degradation tests without a proper control system, it is difficult to comment on the strength retention and its sufficiency in an

*in vivo* condition. Biting forces in the molars for a healthy person can be as high as 250 N on one side. But post fracture treatment of 1 week the forces are as low as 90 N and have seen to increase up to 148 N in 6 weeks [46]. Future design adaptations should make use of biomechanical models offered by softwares such as OpenSim and ANYBODY TECHNOLOGY to design implants as per the biomechanics of the implantation site. These tools account for joint forces, muscle activation and forces and help to simulate activities of daily life, such as chewing and yawning which can then help predict loading situations that can be experimentally performed and help to improve implant design.

### 4.3. *In vitro* tests

#### 4.3.1. Indirect contact assay

In the indirect contact assay, decreasing degree of cell viability was observed with increasing concentration of extracts. Severe cytotoxicity was observed for 100 % extract conditions. This result is similar to the trends observed by J. Fischer et al [47] for cast Mg and Mg4Y (4 % wt. Yttrium) samples tested under similar experimental conditions and quantified by BrdU, which intercalates in DNA strands when cells replicate and is an indicator of cell proliferation. However, the results are different from the results observed for other Mg-Zn-Ca alloys in the literature and can be explained due to the difference in certain parameters. In the indirect contact assay, three important parameters were recognized which may have influences on the results. These are summarized in Table 4.1 and further elaborated below.

- **pH:** By the methodology and results in this section a maximum pH value of 8.31 was noted in the 100 % extract conditions. This was the pH exposed to cells on Day 0 of the test. In the direct contact assay where implants remained in close vicinity of the implant for the same time period of 72 h, it is possible to assume much harsher conditions since the implant actively corrodes. In this condition, a maximum pH of 9.0 was recorded and cells were seen to be alive for the two implant conditions that were degraded by the culture media. If this recorded pH was cytotoxic, it is safe to assume that cells must behave similarly in any kind of assay at this pH. Since cell viability was observed in the direct contact assay after 72 h at a pH of 9, it is safe to assume a pH of 8.31 observed at the start of 100 % extraction was not the real reason that led to cell death. Furthermore, a pH up to 8.5 is commonly used in osteoblast cultures [48].
- **Extraction vehicle and conditions:** The extraction vehicle as recommended by ISO 10993-5 recommends the use of culture media with serum as the extraction vehicle for mammalian cell assays. Xia et al. [49], Sun et al.[50], and Zhang et al.[51], performed the indirect contact assay on various Mg-Zn-Ca alloys and noted no cytotoxic effects. The difference in parameters noted to the experiments recorded in this report is that the extraction vehicle was serum free and the extracts were also centrifuged to remove any micro particles. Liu et al [52] explains very well the influence of BSA and FBS in extraction media and concludes how these serum

Literature	Extraction vehicle	Condition	Quantification
Xia et al	Serum free	Centrifuged	MTT
Sun et al	Serum free	Centrifuged	Neutral red
Zhang et al	Serum free	Centrifuged	Neutral red
Anvari-Yazdi et al	With serum	Centrifuged	MTT & qualitative
This thesis	With serum	Not centrifuged	DNA extraction and qualitative

Table 4.1: Comparison drawn between parameters in the literature with the thesis which could be a possible explanation to the differences in results observed for cytotoxicity in the indirect contact assay.

components lead to faster corrosion thus widening the already known gap between the *in vitro* and *in vivo* conditions. Similarly, Anvari-Yazdi et al [53] assessed pure Mg, Mg-2Zn and Mg-2Zn-xCa alloys in the presence of ASCs and noted no cytotoxic effects. The extracts were prepared in the media containing FBS and were centrifuged to remove macro particles. In the tests performed for this thesis, for indirect and direct contact assay, salt precipitates attached to the culture plate were observed as shown earlier in Figure 3.15. It is interesting to question if these particles in the 100 % extract may have led to reduction in cell proliferation. If this is so, it would explain why researchers often centrifuged their extracts before the indirect assay and explain the differences in results for a similar material.

- **Quantification methods:** Xia et al and Anvari-Yazdi et al, quantified their results using the MTT assay which is now known to show false positive results. MTT and XTT assays, commonly used, are recommended in ISO 10993-6/11 but many researchers have pointed out corrosion products react with Tetrazolium salts present in these assays [11, 47]. Fischer et al compare the MTT assay results against DNA quantification methods like BrdU and highlights the strike contrast.

In this report, the methodology follows an exaggerated condition as recommended by ISO 10993-12 and not a simulated-use extraction as defined in the ISO 10993-12. For the purpose of testing cytotoxicity, a simulated use extraction might be more beneficial to deem the usefulness of the material, whereas a simulated- exaggerated condition can provide important details of tolerance to elemental osmolality that can be used as thresholds, while further developing the material.

#### 4.3.2. Direct contact assay

In the direct contact assay, a major drawback in methodology was observed when the implant was noticed to be moving. This may have introduced shear on the cells and caused a variance in result, thus indicating repetition necessary. Nevertheless, interesting observations were noted for the three implant conditions. For the non degraded implants, well proliferated and viable cells were observed along the edge of the culture well. Some viable cells and few rounded cells were seen in close vicinity of the implant. This result is similar to what Fischer et al observed for pure Mg samples [47]. The low

cell density could be attributed to the movement of the implant or due to disturbance by the actively degrading material. In some cases, bubbles and salt precipitates were observed. At all times, when salt precipitates were observed, viable cells were not observed. In the DMEM degraded implant, viable cells were observed only under the implant. In the rest of the well including the edge of the well, many dead cells were observed. A possible reason for this could be the low corrosion rate on the bottom surface of the implant due to less media reaching the site. In the SBF degraded implant condition, no viable cells and many dead cells were observed in the well. This could be attributed to the concentration of the various salts already present on the implant surface due to the SBF degradation. It could be speculated that some kind of reactions occurs between Mg or corrosion products with phenol red in DMEM that indicates the change of color. No resources could be found explaining this and it is different from the usual pH indication by colour change.

#### 4.3.3. Direct seeding assay

This assay performed as expected for a magnesium sample. When the cell suspension was placed on the implant surface many bubbles (suspected to be hydrogen gas) could be visible to the naked eye. Due to the active surface, it was expected that cells might not attach and this was confirmed in the results. In this assay, only the non degraded and SBF degraded samples were tested and not the DMEM degraded discs. It would be interesting to note if a DMEM degraded sample might show different results due to the initial burst of corrosion having already passed. The SBF samples were expected to behave like the DMEM degraded samples, however the various insoluble salts on the surface of the disc might have hindered attachment.

#### 4.3.4. Overall

The *in vitro* testing of Mg and its alloys are widely debated due to the nature of their corrosion and therefore the applicability of the testing guidelines of the current ISO 10993 standards. From the observations of three tests performed in this thesis, the indirect contact assay would be the most appropriate test to recommend for cytotoxicity testing. In this test it would be interesting to assess cell proliferation in serum free culture conditions, as described in the literature, after removing the small precipitates by centrifuging. While a serum free condition is not comparable to *in vivo*, it would still represent the slow corrosion kinetics observed in various animal studies [1, 25]. The *in vitro* corrosion has been found to be four orders of magnitude faster than *in vivo* conditions [54]. Wang et al [55] recommend 6-10 times dilution of extracts from recommendations in the ISO 10993 standards while performing tests with extracts. The static culture experiments also create harsh micro environments and in the future testing with bioreactors or in culture plates with media flow could be evaluated to simulate blood perfusion and to refresh media, move away degradation products from site and regulate pH, all of which would be expected *in vivo*. It would also be useful to compare ZX10 side by side to other Mg alloys such as the WE43 alloy. Extra-high purity Mg has been implanted *in vivo* in rat femur and has shown to be biocompatible [25]. Similarly, Mg-Zn-Ca sys-



tems such as ZX50 [1] and ZX00 [56] have also shown biocompatibility *in vivo* and ZX10 would be expected to behave in a similar manner. Therefore, the *in vitro* tests need to be modified if comparisons must be drawn to *in vivo* conditions.



## Recommendations for future work

From the discussions in the previous chapter, the following recommendations are enlisted for future consideration.

- From the pull out experiments conducted in this report, it is clear that the next prototype of the screw can be designed with a smaller outer diameter. Future aim should focus on minimal material usage with optimal pull out strengths since it is now established that the ZX10 is suitable to manufacture as screws. The insertion of the screws should also follow standardized methods.
- It would be interesting to test the screws and plates as an assembled system on artificial bone in mechanical tests such as 4 point bending, before and after degradation in SBF. As an assembled system, the degradation at the screw head and plate interface would be interesting to observe, to assess if the corrosion is fast enough to create micro-motions between the parts or if it is protected due to less exposure to fluid. The degraded assembled system will help to identify weak points and assess stability. A comparison with other established Mg systems such as the WE43 will also help establish sufficiency.
- Dynamic loading of the implant system in SBF can provide important information about the effects of mechanical loads on corrosion kinetics. While ZX10 behaves better than other ZX alloys, it still shows some susceptibility to stress corrosion cracking and corrosion fatigue [57] and this would be useful and interesting to evaluate under biomechanical loads. In the future, the SBF refreshment, temperature and pH must be better controlled.
- Computational tools such as biomechanical models available from OpenSim or ANYBODY technologies could be explored to design implants that are site specific by accounting for the anatomical loading. These tools can help avoid issues of over dimensioning.

- In future *in vitro* tests, using a control of WE43 system can provide more concrete conclusions on cell proliferation and viability. Prior decision making on emulating *in vivo* environments with respect to expected nature and quantity of corrosion products (centrifuged and less corrosion products) or the environment itself (with flow and proteins of serums etc.) must be established so as to be able to compare appropriately with literature and other testing conditions. It would be interesting to test, culture media degraded implants by direct seeding assays to assess cell attachment for this predegraded condition and check for differences with SBF degraded and non degraded conditions.
- Apart from cytotoxicity tests, hemocompatibility tests as per ISO 10993-4 could be undertaken, even if the envisioned application is not on the ISO suggested list. This is recommended because the alloy is degrading and the flow of blood is the expected to carry away the corrosion products. Testing with blood will not only provide information on hemolysis, thrombus formation, platelet and coagulation response, but also on the effect of flow, and adsorption of various proteins and lipids on the material surface and thereby their effects on corrosion kinetics.

# 6

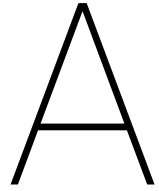
## Conclusion

Overall from the results in this report, the ZX10 alloy is a material with tremendous potential for application in the treatment of mandibular angle fractures. Final conclusions from the work-flow and conclusions on the hypothesis are elaborated below.

- Sample material selection: The manufacturing methods can have a huge impact on material properties and is a vital detail to report while biomedically characterizing a material. The ZX10 alloy can be manufactured suitably to function as implants.
- Implant designing: ZX10 can form suitable implant designs and future work should account for the biomechanics of the application area and be dimensioned optimally.
- Mechanical testing: ZX10 can perform well in the CMF region as compared to commercially available devices but comparisons must be drawn to other biodegrading materials.
- Cytotoxicity testing: ZX10 shows promising results when exposed to cells and degradation products in low concentrations do not produce cytotoxic effects.

ZX10 was hypothesized to perform comparably to commercial systems in terms of mechanical strength while designed in acceptable dimensions and from the results in this report, this hypothesis holds true. The hypothesis regarding cytotoxic effects is held partially true as some conditions of corrosion products (high extract concentration and salt precipitates) have shown to elicit cytotoxic effects. That being said, the effects seen *in vitro* are not absolute representations of *in vivo* situations and further experiments are warranted to generate *in vitro* data that better predict *in vivo* biocompatibility, and to compare ZX10 side-by-side with other Mg alloys.





## Raw material analysis

### **A.1. Fraction of recrystallization**



Front end of the extruded raw material to manufacture screws



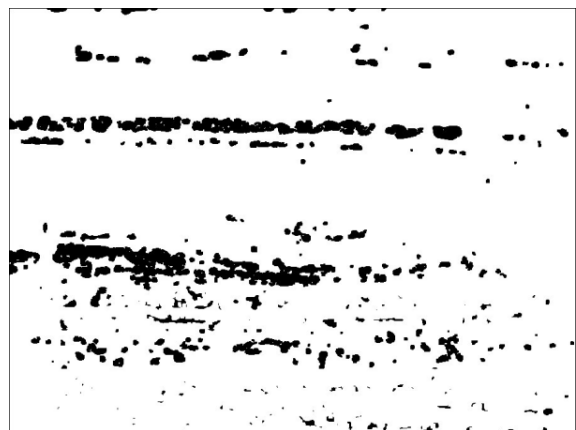
Sample: A12-C02-R1

0 294529

255 313646

Fraction of recrystallization 51.58 %

Rear end of the extruded raw material to manufacture screws



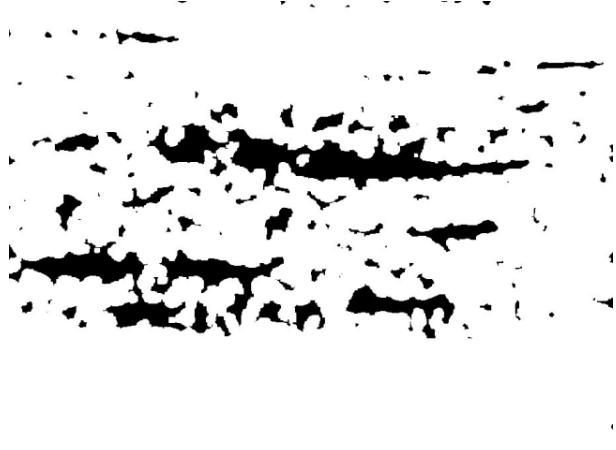
Sample: A12-C02-R5

0 50471

255 557029

Fraction of recrystallization 91.7 %

Front end of the extruded raw material to manufacture plates



Sample: A12-C03-R1

0 61617

255 543855

Fraction of recrystallization 89.83 %

Rear end of the extruded raw material to manufacture plates



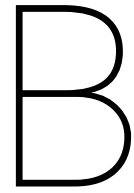
Sample: A12-C03-R6

0 283103

255 324397

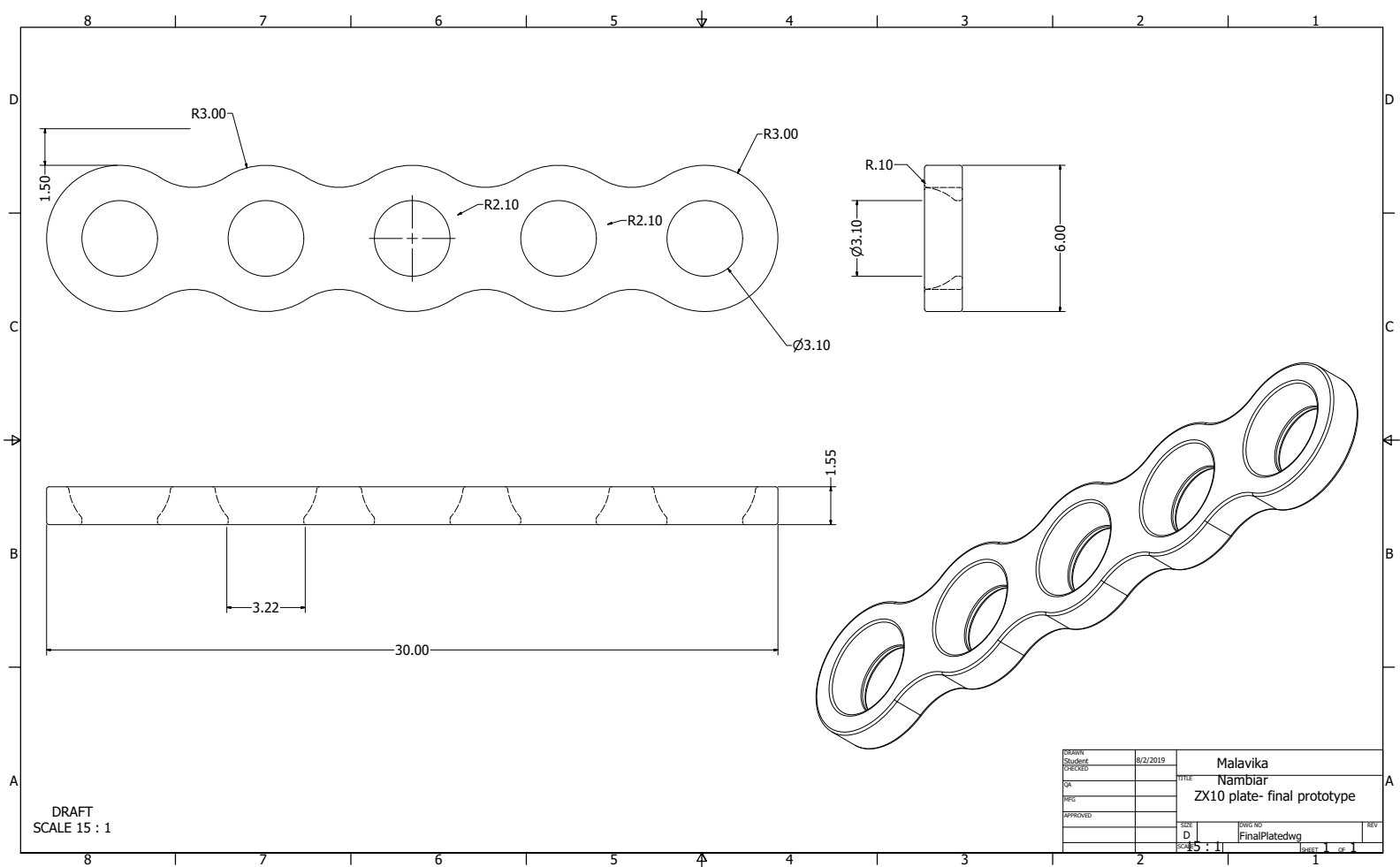
Fraction of recrystallization 53.4 %

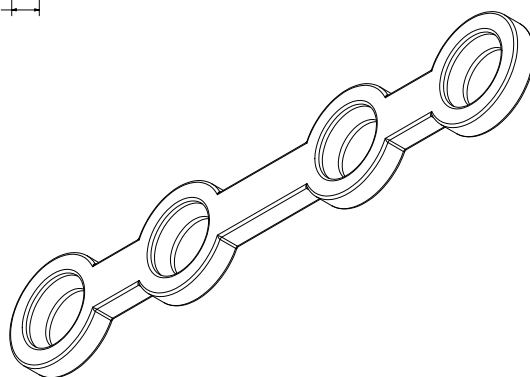
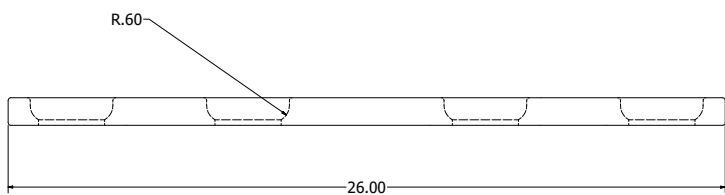
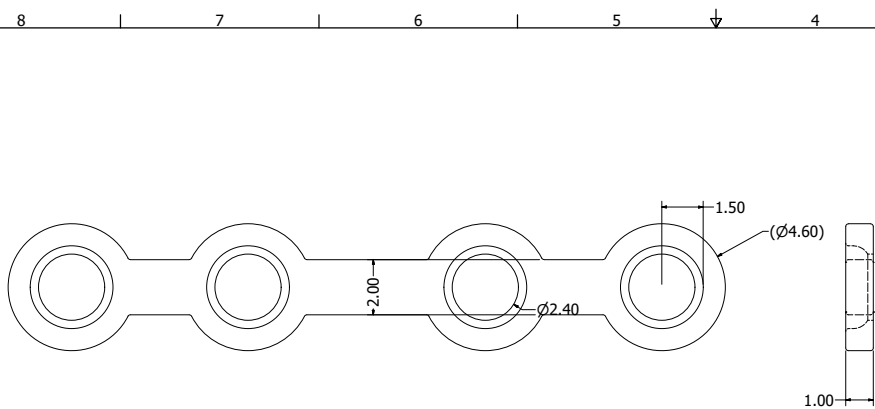




## CAD drawings

Drawing of the CAD files generated on Autodesk Inventor professional for the final manufactured ZX10 implants and the titanium plate model used for FEM are included below.





OSDWN	8/2/2019	Malavika Nambiar	
Student		TITLE	
CHECKED		Ti plate	
QA			
REG			
APPROVED			
		SIZE D	DWG NO 20190426TiPlate
		SCALE 5:1	SHEET OF

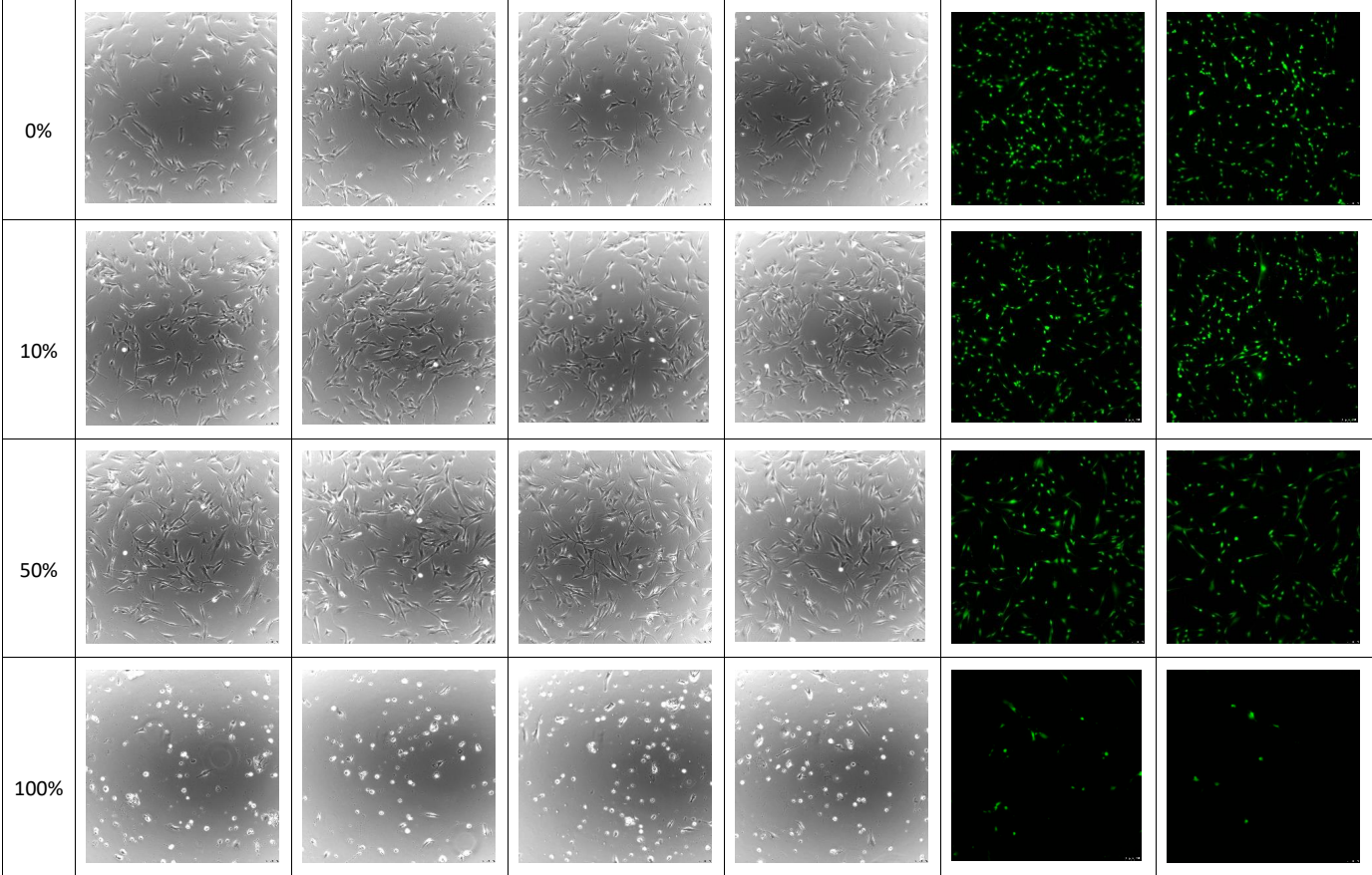




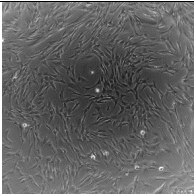
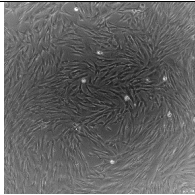
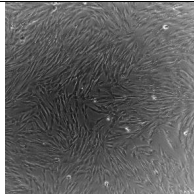
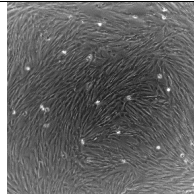
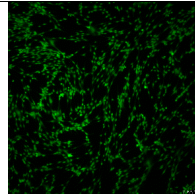
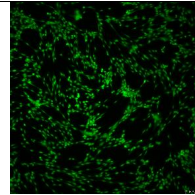
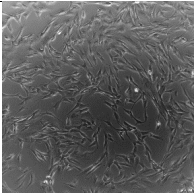
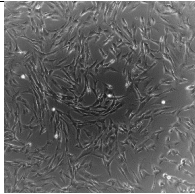
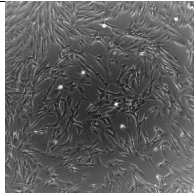
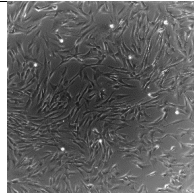
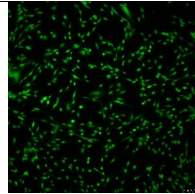
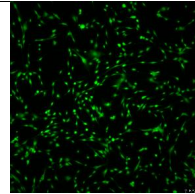
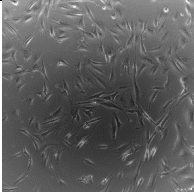
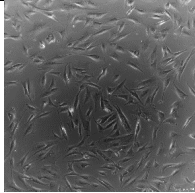
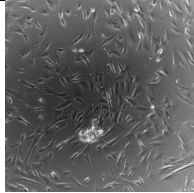
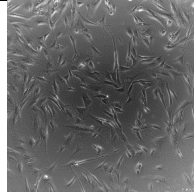
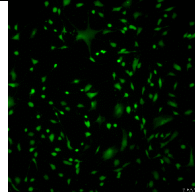
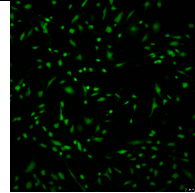

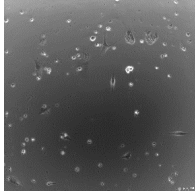
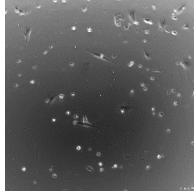
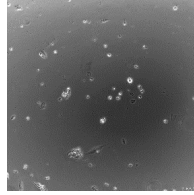
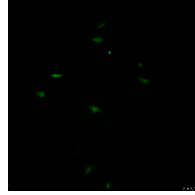
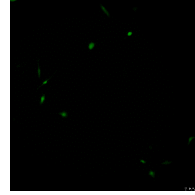
C

## *In vitro* detailed results

The detailed results from each well of the indirect contact experiment are presented below. The 4 wells corresponding to phase contrast are from where the DNA was extracted.



Indirect contact DAY 1 Phase contrast and L/D- Live channel

0%						
10%						
50%						
100 %						

Indirect contact Day 3 Phase contrast and L/D- Live channel



# Bibliography

- [1] J. Hofstetter, E. Martinelli, S. Pogatscher, P. Schmutz, E. Povoden-Karadeniz, A. M. Weinberg, P. J. Uggowitzer, and J. F. Löffler, "Influence of trace impurities on the in vitro and in vivo degradation of biodegradable Mg-5Zn-0.3Ca alloys," *Acta Biomaterialia*, vol. 23, no. May, pp. 347–353, 2015.
- [2] R. Cienfuegos, C.-P. Cornelius, E. Ellis III, and G. Kushner, "Mandible - reduction & fixation - orif, one miniplate - angle and ramus, simple - ao surgery reference." <https://www.aofoundation.org>, accessed 2019-07-17.
- [3] B. M. Pereira, L. G. Fernandez, G. D. Garcia, S. Prichayudt, W. Sánchez, M. d. S. Martins, J. P. Herrera-Escobar, T. Tsunoyama, C. Ordoñez, and G. P. Fraga, "An Overview of Musculoskeletal Injuries for Emergency Physicians," *Emergency Medicine - Open Journal*, vol. 1, no. 3, pp. 77–88, 2015.
- [4] R. M. Slone, R. M. Slone, M. M. Heare, M. M. Heare, R. A. Vander Griend, R. A. Vander Griend, W. J. Montgomery, and W. J. Montgomery, "Orthopedic fixation devices.," *Radiographics : a review publication of the Radiological Society of North America, Inc*, vol. 11, no. 5, pp. 823–847, 1991.
- [5] E. A. Friis, T. A. DeCoster, and J. C. Thomas, *Mechanical testing of fracture fixation devices*. Elsevier Ltd., 2017.
- [6] D. I. Vos and M. H. Verhofstad, "Indications for implant removal after fracture healing: A review of the literature," *European Journal of Trauma and Emergency Surgery*, vol. 39, no. 4, pp. 327–337, 2013.
- [7] G. Reith, V. Schmitz-Greven, K. O. Hensel, M. M. Schneider, T. Tinschmann, B. Bouillon, and C. Probst, "Metal implant removal: benefits and drawbacks - a patient survey," *BMC Surgery*, vol. 15, no. 1, pp. 1–8, 2015.
- [8] W. Jamil, M. Allami, M. Z. Choudhury, C. Mann, T. Bagga, and A. Roberts, "Do orthopaedic surgeons need a policy on the removal of metalwork? A descriptive national survey of practicing surgeons in the United Kingdom," *Injury*, vol. 39, no. 3, pp. 362–367, 2008.
- [9] P. P. Schmittenbecher, "Implant removal in children," *European Journal of Trauma and Emergency Surgery*, vol. 39, no. 4, pp. 345–352, 2013.

- [10] C. Edward Emil Schmitt, Norwalk, "Polyglycolic acid prosthetic devices," 1969.
- [11] E. Willbold, A. Weizbauer, A. Loos, J. M. Seitz, N. Angrisani, H. Windhagen, and J. Reifenrath, "Magnesium alloys: A stony pathway from intensive research to clinical reality. Different test methods and approval-related considerations," *Journal of Biomedical Materials Research - Part A*, vol. 105, no. 1, pp. 329–347, 2017.
- [12] P. Rokkanen, S. Vainionpää, P. Törmälä, J. Kilpikari, O. Böstman, K. Vihtonen, J. Laiho, and M. Tamminmäki, "BIODEGRADABLE IMPLANTS IN FRACTURE FIXATION: EARLY RESULTS OF TREATMENT OF FRACTURES OF THE ANKLE," *The Lancet*, 1985.
- [13] O. Bostman, E. Hirvensalo, J. Makinen, and P. Rokkanen, "Foreign-body reactions to fracture fixation implants of biodegradable synthetic-polymers," *JOURNAL OF BONE AND JOINT SURGERY-BRITISH VOLUME*, vol. 72, pp. 592–596, jul 1990.
- [14] H. J. Helling, A. Prokop, H. U. Schmid, M. Nagel, J. Lilienthal, and K. E. Rehm, "Biodegradable implants versus standard metal fixation for displaced radial head fractures. A prospective, randomized, multicenter study," *Journal of Shoulder and Elbow Surgery*, vol. 15, no. 4, pp. 479–485, 2006.
- [15] T. Nishizuka, T. Kurahashi, T. Hara, H. Hirata, and T. Kasuga, "Novel intramedullary-fixation technique for long bone fragility fractures using bioresorbable materials," *PLoS ONE*, vol. 9, no. 8, 2014.
- [16] P. Balasubramanian, L. A. Strobel, U. Kneser, and A. R. Boccaccini, "Zinc-containing bioactive glasses for bone regeneration, dental and orthopedic applications," *Biomedical Glasses*, vol. 1, no. 1, pp. 51–69, 2015.
- [17] M. H. Emily Walker, "Magnesium, Iron and Zinc Alloys, the Trifecta of Bioresorbable Orthopaedic and Vascular Implantation - A Review," *Journal of Biotechnology & Biomaterials*, vol. 05, no. 02, 2015.
- [18] E. Huse, "A new ligature?," *Chicago Med J Exam*, pp. 172–2, 1878.
- [19] S. V. Verstraeten, L. Aimo, and P. I. Oteiza, "Aluminium and lead: Molecular mechanisms of brain toxicity," *Archives of Toxicology*, vol. 82, no. 11, pp. 789–802, 2008.
- [20] D. Bian, W. Zhou, Y. Liu, N. Li, Y. Zheng, and Z. Sun, "Acta Biomaterialia Fatigue behaviors of HP-Mg, Mg – Ca and Mg – Zn – Ca biodegradable metals in air and simulated body fluid," *Acta Biomaterialia*, vol. 41, pp. 351–360, 2016.
- [21] H. H. Bayraktar, E. F. Morgan, G. L. Niebur, G. E. Morris, E. K. Wong, and T. M. Keaveny, "Comparison of the elastic and yield properties of human femoral trabecular and cortical bone tissue," *Journal of Biomechanics*, vol. 37, no. 1, pp. 27–35, 2004.

- [22] W. J. Seong, U. K. Kim, J. Q. Swift, Y. C. Heo, J. S. Hodges, and C. C. Ko, "Elastic properties and apparent density of human edentulous maxilla and mandible," *International Journal of Oral and Maxillofacial Surgery*, vol. 38, no. 10, pp. 1088–1093, 2009.
- [23] H. Devlin, K. Horner, and D. Ledgerton, "A comparison of maxillary and mandibular bone mineral densities.," *The Journal of prosthetic dentistry*, vol. 79, no. 3, pp. 323–327, 1998.
- [24] J. Hoffstetter, "Influence of Ca and Zn on the microstructure and corrosion of biodegradable Mg-Ca-Zn alloys," *Corrosion Science*, vol. 93, pp. 222–233, apr 2015.
- [25] J. Hofstetter, E. Martinelli, A. M. Weinberg, M. Becker, B. Mingler, P. J. Uggowitzer, and J. F. Löffler, "Assessing the degradation performance of ultrahigh-purity magnesium in vitro and in vivo," *Corrosion Science*, vol. 91, pp. 29–36, 2015.
- [26] J. Hofstetter, S. Rüedi, I. Baumgartner, H. Kilian, B. Mingler, E. Povoden-Karadeniz, S. Pogatscher, P. J. Uggowitzer, and J. F. Löffler, "Processing and microstructure-property relations of high-strength low-alloy (HSLA) Mg-Zn-Ca alloys," *Acta Materialia*, vol. 98, pp. 423–432, 2015.
- [27] M. A. Cabrini Gabrielli, M. F. Real Gabrielli, E. Marcantonio, and E. Hochuli-Vieira, "Fixation of mandibular fractures with 2.0-mm miniplates: Review of 191 cases," *Journal of Oral and Maxillofacial Surgery*, vol. 61, no. 4, pp. 430–436, 2003.
- [28] A. S. Murthy and J. A. Lehman, "Symptomatic plate removal in maxillofacial trauma: A review of 76 cases," *Annals of Plastic Surgery*, vol. 55, no. 6, pp. 603–607, 2005.
- [29] V. Bhatt and R. J. Langford, "Removal of miniplates in maxillofacial surgery: University Hospital Birmingham experience," *Journal of Oral and Maxillofacial Surgery*, vol. 61, no. 5, pp. 553–556, 2003.
- [30] H. Qin, Y. Zhao, M. Cheng, Q. Wang, Q. Wang, J. Wang, Y. Jiang, Z. An, and X. Zhang, "Anti-biofilm properties of magnesium metal via alkaline pH," *RSC Advances*, vol. 5, no. 28, pp. 21434–21444, 2015.
- [31] C. Patussi, L. M. Sassi, R. Cruz, G. Klein Parise, D. Costa, and N. L. B. Rebellato, "Evaluation of different stable internal fixation in unfavorable mandible fractures under finite element analysis," *Oral and Maxillofacial Surgery*, 2019.
- [32] M. Brucoli, P. Boffano, A. Pezzana, A. Benech, P. Corre, H. Bertin, P. Pechalova, N. Pavlov, P. Petrov, T. Tamme, A. Kopchak, A. Romanova, E. Shuminsky, E. Dediol, M. Tarle, V. S. Konstantinovic, D. Jelovac, K. H. Karagozoglu, and T. Forouzanfar, "The "European Mandibular Angle" research project: the analysis of complications after unilateral angle fractures," *Oral Surgery, Oral Medicine, Oral Pathology and Oral Radiology*, vol. 128, no. 1, pp. 14–17, 2019.



- [33] J. C. de Oliveira, L. B. Moura, J. D. de Menezes, M. A. Gabrielli, V. A. Pereira Filho, and E. Hochuli-Vieira, "Three-dimensional strut plate for the treatment of mandibular fractures: a systematic review," *International Journal of Oral and Maxillofacial Surgery*, vol. 47, no. 3, pp. 330–338, 2018.
- [34] J. Hofstetter, S. Rüedi, I. Baumgartner, H. Kilian, B. Mingler, E. Povoden-Karadeniz, S. Pogatscher, P. J. Uggowitzer, and J. F. Löffler, "Processing and microstructure-property relations of high-strength low-alloy (HSLA) Mg-Zn-Ca alloys," *Acta Materialia*, vol. 98, pp. 423–432, 2015.
- [35] A. I. (2006), "Standard Specification for Unalloyed Titanium, for Surgical Implant Applications (UNS R50250, UNS R50400, UNS R50550, UNS R50700)."
- [36] C. Elias, J. Lima, R. Valiev, and M. Meyers, "Biomedical applications of titanium and its alloys Biological Materials Science 46-49," *Biological Materials Science*, no. March, pp. 1–4, 2008.
- [37] M. Kozakiewicz and P. Sołtysiak, "Pullout force comparison of selected screws for rigid fixation in maxillofacial surgery," *Dental and Medical Problems*, vol. 54, no. 2, pp. 129–133, 2017.
- [38] M. Schinhammer, J. Hofstetter, C. Wegmann, F. Moszner, J. F. Löffler, and P. J. Uggowitzer, "On the immersion testing of degradable implant materials in simulated body fluid: Active pH regulation using CO<sub>2</sub>," *Advanced Engineering Materials*, vol. 15, no. 6, pp. 434–441, 2013.
- [39] "International Standard ISO 10993-5," vol. Third edition, 2009.
- [40] J. C. Shelton and R. A. Loukota, "Pull-out strength of screws from cortical bone in the maxillofacial region," *Journal of Materials Science: Materials in Medicine*, vol. 7, no. 4, pp. 231–235, 1996.
- [41] SAWBONES, "General catalog pg. 80." [https://www.sawbones.com/media/assets/product/documents/general\\_catalog.pdf](https://www.sawbones.com/media/assets/product/documents/general_catalog.pdf), accessed 2019-07-01.
- [42] R. M. Laughlin, M. S. Block, R. Wilk, R. B. Malloy, and J. N. Kent, "Resorbable Plates for the Fixation of Mandibular Fractures: A Prospective Study," *Journal of Oral and Maxillofacial Surgery*, vol. 65, no. 1, pp. 89–96, 2007.
- [43] J. O. Dow, "Shear Locking, Aspect Ratio Stiffening, and Qualitative Errors," *A Unified Approach to the Finite Element Method and Error Analysis Procedures*, pp. 271–305, 2007.
- [44] W. D. Mueller, M. Lucia Nascimento, and M. F. Lorenzo De Mele, "Critical discussion of the results from different corrosion studies of Mg and Mg alloys for biomaterial applications," *Acta Biomaterialia*, vol. 6, no. 5, pp. 1749–1755, 2010.

- [45] T. Imwinkelried, S. Beck, T. Iizuka, and B. Schaller, "Effect of a plasmaelectrolytic coating on the strength retention of in vivo and in vitro degraded magnesium implants," *Acta Biomaterialia*, vol. 9, no. 10, pp. 8643–8649, 2013.
- [46] K. L. Gerlach and A. Schwarz, "Bite forces in patients after treatment of mandibular angle fractures with miniplate osteosynthesis according to Champy," *International Journal of Oral and Maxillofacial Surgery*, vol. 31, no. 4, pp. 345–348, 2002.
- [47] M. J. Fischer, Wolff, R. Willumeit, F. Feyerabend, J. Fischer, M. H. Prosenc, and N. Hort, "Interference of magnesium corrosion with tetrazolium-based cytotoxicity assays," *Acta Biomaterialia*, vol. 6, no. 5, pp. 1813–1823, 2009.
- [48] N. A. Agha, R. Willumeit-römer, and D. Laipple, "The Degradation Interface of Magnesium Based Alloys in Direct Contact with Human Primary Osteoblast Cells," *PLoS ONE*, pp. 1–20, 2016.
- [49] Y. Xia, B. Zhang, Y. Wang, M. Qian, and L. Geng, "In-vitro cytotoxicity and in-vivo biocompatibility of as-extruded Mg-4.0Zn-0.2Ca alloy," *Materials Science and Engineering C*, vol. 32, no. 4, pp. 665–669, 2012.
- [50] Y. Sun, B. Zhang, Y. Wang, L. Geng, and X. Jiao, "Preparation and characterization of a new biomedical Mg-Zn-Ca alloy," *Materials and Design*, vol. 34, pp. 58–64, 2012.
- [51] B. Zhang, Y. Hou, X. Wang, Y. Wang, and L. Geng, "Mechanical properties, degradation performance and cytotoxicity of Mg-Zn-Ca biomedical alloys with different compositions," *Materials Science and Engineering C*, vol. 31, no. 8, pp. 1667–1673, 2011.
- [52] X. Liu, T. Xi, and Y. Zheng, "Influence of the extraction parameters on the cytotoxicity test results of Mg materials," *Progress in Natural Science: Materials International*, vol. 24, no. 5, pp. 507–515, 2014.
- [53] A. Fazel Anvari-Yazdi, K. Tahermanesh, S. M. M. Hadavi, T. Talaei-Khozani, M. Razmkhah, S. M. Abed, and M. S. Mohtasebi, "Cytotoxicity assessment of adipose-derived mesenchymal stem cells on synthesized biodegradable Mg-Zn-Ca alloys," *Materials science & engineering. C, Materials for biological applications*, vol. 69, pp. 584–597, dec 2016.
- [54] F. Witte, J. Fischer, J. Nellesen, H.-A. Crostack, V. Kaese, A. Pisch, F. Beckmann, and H. Windhagen, "In vitro and in vivo corrosion measurements of magnesium alloys," *Biomaterials*, vol. 27, no. 7, pp. 1013–8, 2006.
- [55] J. Wang, F. Witte, T. Xi, Y. Zheng, K. Yang, Y. Yang, D. Zhao, J. Meng, Y. Li, W. Li, K. Chan, and L. Qin, "Recommendation for modifying current cytotoxicity testing standards for biodegradable magnesium-based materials," *Acta Biomaterialia*, vol. 21, pp. 237–249, 2015.

- [56] N. G. Grün, P. Holweg, S. Tangl, J. Eichler, L. Berger, J. J. van den Beucken, J. F. Löffler, T. Klestil, and A. M. Weinberg, "Comparison of a resorbable magnesium implant in small and large growing-animal models," *Acta Biomaterialia*, vol. 78, pp. 378–386, 2018.
- [57] S. Jafari, R. K. Raman, C. H. Davies, J. Hofstetter, P. J. Uggowitzer, and J. F. Löffler, "Stress corrosion cracking and corrosion fatigue characterisation of MgZn1Ca0.3 (ZX10) in a simulated physiological environment," *Journal of the Mechanical Behavior of Biomedical Materials*, vol. 65, no. September 2016, pp. 634–643, 2017.

